Extended Chirp Scaling-Baseband Azimuth Scaling based Azimuth-Range Decouple L_1 Regularization for TOPS SAR Imaging via CAMP

Hui Bi, Bingchen Zhang, Xiao Xiang Zhu, *Senior Member, IEEE,*
Chenglong Jiang, and Wen Hong, *Member, IEEE*

***Abstract*—This paper proposes a novel azimuth-range decouple based L_1 regularization imaging approach for the focusing in Terrain Observation by Progressive Scans (TOPS) synthetic aperture radar (SAR). Due to conventional L_1 regularization technique requires transferring the two-dimensional (2-D) echo data into a vector and reconstructing the scene via 2-D matrix operations leading to significantly more computational complexity, it very difficult to apply in high-resolution and wide-swath SAR imaging, *e.g.*, TOPS. The proposed method can achieve azimuth-range decouple by constructing an approximated observation operator to simulate the raw data, the inverse of matching filtering (MF) procedure, which makes large-scale sparse reconstruction, or called compressive sensing (CS) reconstruction of surveillance region with full- or down-sampled raw data in TOPS SAR possible. Compared to MF algorithm, *e.g.*, extended chirp scaling-baseband azimuth scaling (ECS-BAS), it shows huge potential in image performance improvement. While compared with conventional L_1 regularization technique, it significantly reduces the computational cost, and provides similar image features. Furthermore, this novel approach also can obtain a non-sparse estimation of considered scene retaining a similar background statistical distribution as MF based image, which can be used to the further application of SAR images with precondition being a preserving image statistical properties, *e.g.*, constant false alarm rate detection (CFAR). Experimental results along with a performance analysis validate the proposed method.**

***Index Terms*—Synthetic aperture radar (SAR), terrain observation by progressive scans (TOPS), extended chirp scaling (ECS), baseband azimuth scaling (BAS), azimuth-range decouple, L_1 regularization, complex approximated message passing (CAMP).**

I. INTRODUCTION

IN modern synthetic aperture radar (SAR) processing [1], wide-swath imaging is one of the most important development trends which has been commonly used in marine monitoring, ship detection, *etc*. Terrain Observation by Progressive Scans (TOPS) is a novel wide-swath SAR imaging mode which increases the swath by periodically switching the incidence angle of antenna among different subswaths from near to far range [2], [3]. Compared to ScanSAR [4], the other typical wide-swath mode, TOPS can overcome the problems of scalloping and azimuth varying signal-to-ambiguity ratio efficiently through steering the antenna mechanically or electronically in the along-track direction [5].

Chirp scaling [6], [7] is a well-known matching filtering (MF) based SAR focusing algorithm, which can obtain high-resolution SAR image without using interpolation operation, and hence has been widely used in Stripmap [8], [9] and Spotlight [10], [11] modes. In 1996, Moreira *et al.* have developed an extended chirp scaling (ECS) algorithm [12] for ScanSAR imaging by achieving azimuth scaling with Spectral Analysis (SPECAN) technique [13], and further applied ECS to Stripmap [12] and Spotlight [14] SAR successfully. For TOPS, Prats *et al.* proposed a baseband azimuth scaling (BAS) algorithm in 2010 [5], which extends the conventional ECS approach, utilizes the sub-aperture technique to resolve the aliased Doppler spectra without interpolation, and hence obtains high-resolution TOPS SAR image. In these years, several algorithms have been proposed and show exciting performance in raw data processing of TOPS [15]- [20]. Generally, above-mentioned existing TOPS SAR imaging methods are computationally efficient, but may suffer severely from clutter and sidelobes, which restrict their application in target identification, feature extraction, *etc*.

Compressive sensing (CS) [21], [22], an important development in sparse signal processing, was proposed by Donoho *et al.* in 2006. CS theory shows that, if measurement matrix satisfies some conditions, *e.g.*, restricted isometry property (RIP) [23], original sparse signals can be recovered from far less samples than the well-known Shannon-Nyquist sampling theory requires [24], [25]. Baraniuk and Steeghs first introduced CS to radar imaging in 2007 [26]. Then sparse reconstruction was widely used and led to promising results in radar signal processing, *e.g.*, synthetic aperture radar tomography (TomoSAR) [27], inverse synthetic aperture radar (ISAR) [28], and multiple input multiple output (MIMO) [29]. Certainly, sparse signal processing technique also can be

---

Manuscript received xxxx xx, 2016; revised xxxx xx, 2016; accepted xxxx xx, 2017. This work was supported by the Chinese Academy of Sciences/State Administration of Foreign Experts Affairs (CAS/SAFEA) International Partnership Program for Creative Research Team, and the National Natural Science Foundation of China under Grant 61571419.

H. Bi is with the Science and Technology on Microwave Imaging Laboratory, Institute of Electronics, Chinese Academy of Sciences, Beijing 100190, China, and also with the University of Chinese Academy of Sciences (UCAS), Beijing 100049, China (e-mail: bihui1991@163.com).

B. Zhang, C. Jiang, and W. Hong are with the Science and Technology on Microwave Imaging Laboratory, Institute of Electronics, Chinese Academy of Sciences, Beijing 100190, China (e-mail: bczhang@mail.ie.ac.cn; jiangcl@live.com; whong@mail.ie.ac.cn).

X. X. Zhu is with the Remote Sensing Technology Institute (IMF), German Aerospace Center (DLR), Oberpfaffenhofen, Wessling 82234, Germany, and also with the Signal Processing in Earth Observation (SiPEO), Technische Universität München (TUM), Munich 80333, Germany (e-mail:xiao.zhu@dlr.de).

applied to SAR imaging. In 2012, Zhang *et al.* demonstrated this combination, called sparse microwave imaging, and reconstructed the surveillance region by solving a $L_q\,(0 \leq q \leq 1)$ regularization problem [30]. Then Çetin *et al.* summarized the development of sparsity-driven SAR imaging in 2014 [31]. Compared to MF based SAR imaging techniques, it can improve the recovered image quality efficiently [32]. However, due to azimuth and range directions are coupled in raw data domain, conventional L_q regularization methods need to transfer the two-dimensional (2-D) raw data into a vector before reconstruction, which is time-consuming and produces significant computational complexity, hence is very difficult to apply in practical large-scale imaging. To solve this problem, Zhang *et al.* proposed an azimuth-range decouple based L_q regularization SAR imaging idea to reduce the computational cost [30], and applied this concept to Stripmap and ScanSAR imaging successfully [33], [34]. This method decouples azimuth and range couple by constructing an approximated observation operator to simulate the raw data, the inverse of MF procedure, and hence relieves the computational pressure compared with conventional L_q regularization technique.

Complex approximated message passing (CAMP), a L_1 regularization recovery algorithm, was proposed by Maleki *et al.* [35]- [37]. Compared to other L_q regularization recovery algorithms, *e.g.*, iterative thresholding algorithm (ITA) [38], orthogonal matching pursuit (OMP) [39], CAMP can not only obtain a sparse image of considered scene, but also a non-sparse estimation of surveillance region with background statistical properties similar to the MF based result, and hence can be used for further application of S AR image which precondition is the preserving image statistical distribution, *e.g.*, constant false alarm rate (CFAR) detection [37].

In this paper, the main constructions are that we propose a novel azimuth-range decouple based L_1 regularization TOPS SAR imaging mechanism, and successfully apply it to the large-scale sparse reconstruction of considered scene from raw data. In the proposed method, we use the echo simulation operator constructed based on ECS-BAS algorithm to replace the exact observation (measurement matrix) in conventional L_1 regularization based TOPS SAR imaging, where the construction of a high dimensional measurement matrix can be avoided, and then utilize the CAMP algorithm to recover the considered scene from the observations by means of the constructed echo simulation operator. For clarity, the proposed method is denoted as L1-ECS-BAS-CAMP. Compare to MF based imaging approaches, the proposed method can improve the image performance efficiently, *e.g.*, sidelobes reduction, clutter suppression, and down-sampling reconstruction for sparse scene. While compared to conventional L_1 regularization recovery technique, it can significantly reduce computational cost, and achieve similar recovered image quality. This method makes large-scale regularization reconstruction, or called CS reconstruction, of surveillance region in TOPS SAR with full- or down-sampled raw data become possible. In addition, since CAMP recovered non-sparse image preserves the background statistical distribution as MF based result, thus it can be further used for the image statistical property based applications.

The rest of this paper is organized as follows. Section II provides a brief introduction of ECS-BAS algorithm. Then conventional L_1 regularization based TOPS SAR imaging scheme along with a CAMP iterative recovery for one-dimensional (1-D) signal are demonstrated in Section III. Section IV presents the proposed method detailedly form model construction, azimuth-range decouple principle, algorithm derivation, parameter setting, to computational cost analysis. Section V provides the experimental results based on simulated data along with a comprehensive performance analysis in Section VI. The reconstruction of non-sparse scene is shown in Section VII. And conclusions are draw in Section VII with several useful remarks.

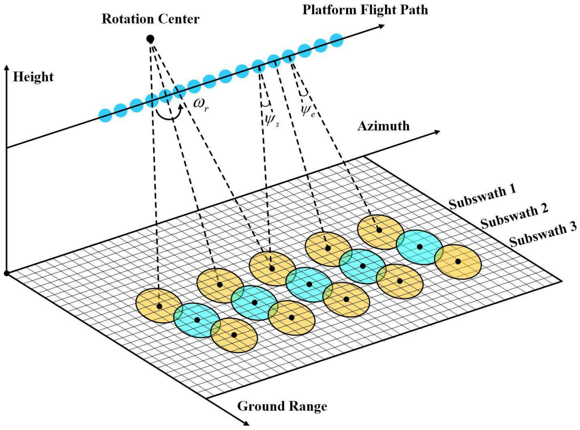

Fig. 1. TOPS SAR imaging geometry.

II. EXTENDED CHIRP SCALING-BASEBAND AZIMUTH SCALING

As shown in Fig. 1, TOPS SAR exploits the burst working mechanism. Thus the baseband echo data $y(\eta,\tau)$ at time (η,τ) can be expressed as

$$\begin{aligned} y(\eta,\tau) = & \iint\limits_{(p,q)\,\in\,\mathbb{C}^b} x(p,q)\cdot \mathrm{rect}\left(\frac{\eta}{T_b}\right) \\ & \cdot\ \omega_a\left(\frac{(\eta - p/v_r) - \eta_c(\eta)}{T_{obs}}\right) \\ & \cdot\ \exp\left\{-j\frac{4\pi}{\lambda}r\right\}\cdot s\left(\tau - \frac{2r}{c}\right) dpdq. \end{aligned} \tag{1}$$

The meaning of parameters are as follows.

η	*Azimuth time*
τ	*Range time*
p	*Target azimuth position*, $1 \leq p \leq N_P$
q	*Target ground range position*, $1 \leq q \leq N_Q$
$x(p,q)$	*Backscattered coefficient at point* (p,q)
λ	*Wavelength*
$\omega_a(\cdot)$	*Antenna azimuth weighting*
c	*Light speed*

v_r	$Platform\ velocity$
T_b	$Burst\ duration$
T_{obs}	$Signal\ cycle\ period$
$\eta_c\left(\eta\right)$	$Beam\ center\ crossing\ time$
$s\left(\tau\right)$	$Transmitted\ pulse\ signal$
H_r	$Relative\ altitude\ of\ platform$
r	$Slant\ range\ with$ $r\left(p,q,\eta\right)=\sqrt{{H_r}^2+q^2+\left(p-v_r\eta\right)^2}$

In BAS [5], the data should be divided in several subapertures whose size satisfy

$$T_{sub}\leqslant\frac{PRF-B_a}{k_{rot}} \tag{2}$$

where B_a is the processed azimuth bandwidth, and k_{rot} is the instantaneous Doppler centroid varying rate. Then the echo data in (1) of one point target can be rewritten as

$$\begin{aligned} y\left(\eta,\tau\right) &= x\left(p,q\right)\cdot\mathrm{rect}\left(\frac{\eta}{T_b}\right)\cdot\mathrm{rect}\left(\frac{\eta-\eta_{sub}}{T_{sub}}\right)\\ &\cdot\ \omega_a\left(\frac{\left(\eta-p/v_r\right)-\eta_c\left(\eta\right)}{T_{obs}}\right)\\ &\cdot\ \exp\left\{-j\frac{4\pi}{\lambda}r\right\}\cdot s\left(\tau-\frac{2r}{c}\right) \end{aligned} \tag{3}$$

where $\eta_{sub}=p/v_f$ with v_f being the footprint velocity.

Let operator $\mathcal{R}\left(\cdot\right)$ indicate the ECS-BAS imaging procedure [5], [12], which flow diagram is depicted in the upper row of Fig. 2. The definition of several operators used in ECS-BAS are listed as following.

$\mathbf{F}_r$	$Range\ Fourier\ transform$
$\mathbf{F}_a$	$Azimuth\ Fourier\ transform$
$\mathbf{F}_r^{-1}$	$Range\ inverse\ Fourier\ transform$
$\mathbf{F}_a^{-1}$	$Azimuth\ inverse\ Fourier\ transform$
$\mathbf{\Gamma}_{sub}$	$Sub-aperture\ division$
$\mathbf{\Gamma}_{sum}$	$Sub-aperture\ recombination$
$\mathbf{\Theta}_1$	$Chirp\ scaling\ operation\ matrix$
$\mathbf{\Theta}_2$	$RCMC,\ SRC,\ Range\ compression\ operation\ matrix$
$\mathbf{\Theta}_3$	$Phase\ correction\ operation\ matrix$
$\mathbf{\Theta}_4$	$Replace\ hyperbolic\ azimuth\ phase\ with\ quadratic\ phase\ operation\ matrix$
$\mathbf{\Theta}_5$	$De-rotation\ operation\ matrix$
$\mathbf{\Theta}_6$	$Azimuth\ compression\ and\ weighting\ operation\ matrix$
$\mathbf{\Theta}_7$	$Phase\ preservation\ operation\ matrix$

In ECS-BAS, after sub-aperture division, using chirp signal as the transmitted pulse $s\left(\tau\right)$, chirp scaling operation matrix $\mathbf{\Theta}_1$, bulk range cell migration correction (RCMC), secondary range compression (SRC), and range compression operation matrix $\mathbf{\Theta}_2$, and phase correction operation matrix $\mathbf{\Theta}_3$ can be represented as

$$\begin{aligned} &\mathbf{\Theta}_1\left(f_\eta,\tau\right) \ = \\ &\exp\left\{j\pi K_s\left(f_\eta;r_{\mathrm{ref}}\right)C\left(f_\eta\right)\left(\tau-\frac{\tau_{\mathrm{ref}}}{D\left(f_{\eta,V_{r_{\mathrm{ref}}}}\right)}\right)^2\right\} \end{aligned} \tag{4}$$

$$\begin{aligned} \mathbf{\Theta}_2\left(f_\eta,f_\tau\right) &= \exp\left\{j\pi\frac{f_\tau^2}{K_s\left(f_\eta;r_{\mathrm{ref}}\right)\cdot\left[1+C\left(f_\eta\right)\right]}\right\}\\ &\cdot\ \exp\left\{j4\pi\frac{r_{\mathrm{ref}}C\left(f_\eta\right)}{cD\left(f_{\eta_{\mathrm{ref}}},V_{r_{\mathrm{ref}}}\right)}f_\tau\right\} \end{aligned} \tag{5}$$

$$\begin{aligned} &\mathbf{\Theta}_3\left(f_\eta,\tau\right) \ = \\ &\exp\left\{-j\pi\frac{K_s\left(f_\eta,r_{\mathrm{ref}}\right)\left[1+C\left(f_\eta\right)\right]C_s\left(f_\eta\right)}{D^2\left(f_{\eta_{\mathrm{ref}}},V_{r_{\mathrm{ref}}}\right)}\left(\tau-\tau_{\mathrm{ref}}\right)^2\right\} \end{aligned} \tag{6}$$

where f_η and f_τ are the azimuth and range frequency, respectively; r_{ref} is the reference slant range; τ_{ref} is the range time corresponding to r_{ref}; r_0 is the nearest range; $f_0=c/\lambda$ is the carrier frequency; and $K_s\left(f_\eta;r_{\mathrm{ref}}\right)$ is the modified modulation rate of chirp signal which can be expressed as

$$K_s\left(f_\eta;r\right) = \frac{K_r}{1-K_r\frac{cr_0f_\eta^2}{2V_r^2f_0^3D^3\left(f_\eta,V_r\right)}} \tag{7}$$

with

$$D\left(f_\eta,V_r\right) = \sqrt{1-\left(\frac{f_\eta\lambda}{2V_r}\right)^2} \tag{8}$$

and the chirp scaling factor $C\left(f_\eta\right)$ being

$$C\left(f_\eta\right) = \frac{D\left(f_{\eta_{\mathrm{ref}}},V_{r_{\mathrm{ref}}}\right)}{D\left(f_\eta,V_{r_{\mathrm{ref}}}\right)}-1. \tag{9}$$

After above three operations, BAS will replace the hyperbolic azimuth phase with a quadratic phase by using

$$\mathbf{\Theta}_4\left(f_\eta,\tau\right) = \exp\left\{j4\pi\frac{r_0f_0D\left(f_\eta,V_r\right)}{c}\right\}\cdot\exp\left\{-j\pi\frac{{f_\eta}^2}{K_{\mathrm{scl}}}\right\} \tag{10}$$

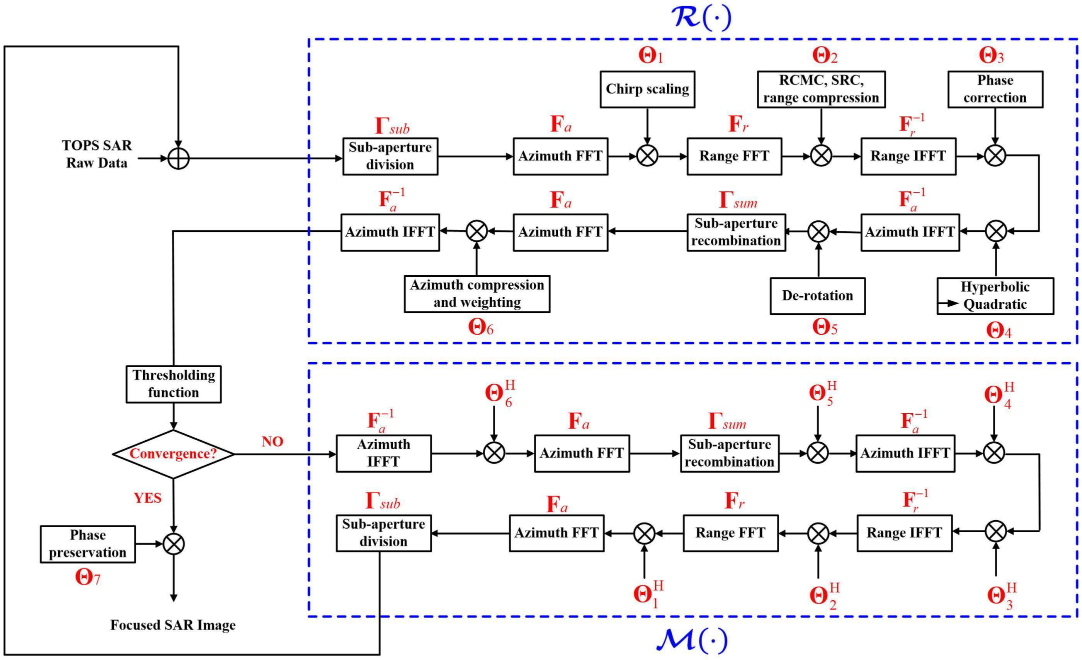

Fig. 2. Flow diagram of the proposed L1-ECS-BAS-CAMP TOPS SAR imaging method.

where the scaling Doppler rate is

$$K_{\text{scl}} = -\frac{2v_{r_{\text{ref}}}^2}{\lambda r_{\text{scl}}(r_0)} \tag{11}$$

where $v_{r_{\text{ref}}}$ is the effective velocity at reference range, $r_{\text{scl}}(r_0)$ is a function of slant range r_0 with $r_0 = \sqrt{H^2+q^2}$. Due to the time at scene center is zero, the demodulation can be performed based on the following de-rotation function

$$\boldsymbol{\Theta}_5(\eta, r_0) = \exp\left\{-j\pi K_{\text{rot}}(r_0)\,\eta^2\right\} \tag{12}$$

with $K_{\text{rot}}(r_0) = -2v_r^2/\lambda r_{\text{rot}}(r_0)$.

In the next, the individual subapertures will be assembled. At this time, the effective chirp rate will be changed from $K_{\text{rot}}(r_0)$ to $K_{\text{eff}}(r_0) = K_{\text{scl}}(r_0) - K_{\text{rot}}(r_0)$. After above operations, azimuth compression and weighting will be done based on the matrix

$$\boldsymbol{\Theta}_6(f_\eta, r_0) = W(f_\eta)\cdot\exp\left\{j\pi\frac{1}{K_{\text{eff}}}f_\eta^2\right\} \tag{13}$$

with $W(f_\eta)$ being the weighting function. Finally, matrix

$$\boldsymbol{\Theta}_7(\eta, r_0) = \exp\left\{-j\pi\frac{2v_{r_{\text{ref}}}^2}{\lambda\left(r_{\text{rot}}(r_0)-r_{\text{scl}}(r_0)\right)}\cdot\left(1-\frac{r_{\text{scl0}}}{r_{\text{rot0}}}\right)^2\cdot\eta^2\right\} \tag{14}$$

is used for phase preserving, where r_{rot0} is the distance to the rotation center which has a fixed value when the scaling range equals to the range of target, and r_{slc0} is a scaling range decided by the azimuth sampling. The scaling vector $r_{\text{scl}}(r_0)$ and rotation vector $r_{\text{rot}}(r_0)$ satisfy

$$r_{\text{scl}}(r_0) = \frac{r_{\text{scl0}}}{r_{\text{rot0}}}r_{\text{rot}}(r_0) \tag{15}$$

and

$$r_{\text{rot}}(r_0) = \frac{r_{\text{rot0}}-r_0}{1-r_{\text{scl0}}/r_{\text{rot0}}}. \tag{16}$$

After performing above operations based on $\boldsymbol{\Theta}_1 \sim \boldsymbol{\Theta}_7$, we can obtain the focused TOPS SAR image.

III. CAMP FOR L_1 REGULARIZATION BASED TOPS SAR IMAGING

In this section, we focus on the conventional L_1 regularization based TOPS SAR imaging including the general formalization of imaging model, with detailed introduction of a CAMP iterative algorithm for L_1 regularization reconstruction.

A. TOPS SAR Imaging Model

We assume the surveillance region is rectangular, with N_P pixels in azimuth and N_Q pixels in range, and characterize a point by its 2-D index (p,q). Let $\mathbf{X}$ denote a $N_P \times N_Q$ matrix whose (p,q) entry is $x(p,q)$, and $\mathbf{x} = \text{vec}(\mathbf{X}) \in \mathbb{C}^{N\times 1}$, where the operation $\text{vec}(\cdot)$ stacks the columns one after the other. Let $\lfloor a \rfloor$ represents the floor of a nonnegative real number

a. For $1 \le n \le N$ with $N = N_P \times N_Q$, define

$$\begin{aligned} p_n &= \lfloor (n-1)/N_P \rfloor + 1 \\ q_n &= n - (p_n - 1)\, N_P. \end{aligned} \tag{17}$$

The nth entry of $\mathbf{x}$ is then $x\,(p_n, q_n)$.

According to the imaging model (1), we discrete the time series as $T_m\,(m = 1, 2, \cdots, M)$. Let $\mathbf{Y} \in \mathbb{C}^{N_\eta \times N_\tau}$ represent the 2-D echo data, and $\mathbf{y} = \mathrm{vec}\,(\mathbf{Y}) \in \mathbb{C}^{M \times 1}$ with $M = N_\eta \times N_\tau$. Thus we can obtain the discretized model as

$$\mathbf{y} \;=\; \sum_{m=1}^{M} \sum_{n=1}^{N} H\,(m,n)\, x\,(p_n, q_n) \tag{18}$$

where TOPS SAR observation matrix $\mathbf{H} \cong \{H\,(m,n)\}_{M \times N}$ represents the imaging geometry relationship between radar and surveillance region, which can be expressed as

$$\begin{aligned} H\,(m,n) \;=\; & \iint\limits_{(\eta,\tau)\,\in\, T_m} \mathrm{rect}\left(\frac{\eta}{T_b}\right) \cdot \omega_a \left(\frac{(\eta - p/v) - \eta_c\,(\eta)}{T_{obs}}\right) \\ \cdot \quad & \exp\left\{-j\frac{4\pi}{\lambda} r\right\} \cdot s\left(\tau - \frac{2r}{c}\right) d\eta d\tau. \end{aligned} \tag{19}$$

Therefore, TOPS SAR imaging model of one burst without down-sampling can be rewritten as

$$\mathbf{y} \;=\; \mathbf{H}\mathbf{x} \;+\; \mathbf{n}_0 \tag{20}$$

where $\mathbf{n}_0 \in \mathbb{C}^{M \times 1}$ is the noise vector. Let $\boldsymbol{\Psi} \cong \{\psi_m\} \in \mathbb{C}^{L \times M}$, $L \le M$ denote the sampling matrix, then the down-sampled 1-D echo data $\mathbf{y}_d \in \mathbb{C}^{L \times 1}$ is

$$\mathbf{y}_d \;=\; \boldsymbol{\Psi}\mathbf{H}\mathbf{x} \;+\; \mathbf{n}_0 \;=\; \boldsymbol{\Phi}\mathbf{x} \;+\; \mathbf{n}_0 \tag{21}$$

where $\boldsymbol{\Phi} \cong \{\phi\,(l,n)\}_{L \times N}$ is the 1-D L_q regularization based SAR imaging measurement matrix which can be expressed as

$$\begin{aligned} \phi\,(l,n) \;=\; & \iint\limits_{(\eta,\tau)\,\in\, T_m} \mathrm{rect}\left(\frac{\eta}{T_b}\right) \cdot \omega_a \left(\frac{(\eta - p/v) - \eta_c\,(\eta)}{T_{\mathrm{obs}}}\right) \\ \cdot \quad & \exp\left\{-j\frac{4\pi}{\lambda} r\right\} \cdot s\left(\tau - \frac{2r}{c}\right) \cdot \psi_m\,(\eta,\tau)\, d\eta d\tau. \end{aligned} \tag{22}$$

If $L = M$, then $\boldsymbol{\Psi}$ is an identity matrix, *i.e.*, there is no down-sampling for the echo data.

In TOPS, the rotation of antenna will reduce the observation time of target. Therefore, we have $\|p\| \le T_s v_r$ with

$$T_s \;=\; (\omega_r T_b + \lambda/L_a)\, \sqrt{H^2 + q^2}\Big/ v_r \;+\; T_b \tag{23}$$

where ω_r is the antenna rotation rate, and L_a is the antenna size. In T_s, only the targets in $\left[-\frac{T_{se}}{2}, \frac{T_{se}}{2}\right]$ with $T_{se} = T_s - 2\frac{\lambda}{L_a}\frac{r}{v_r}$ have the all-aperture echo data and can be achieved regularization reconstruction based on the imaging model (21).

B. L_1 *Regularization Reconstruction*

Since (21) is an under-determined linear system when $L < M$, if $\mathbf{x}$ is sparse enough and $\boldsymbol{\Phi}$ satisfies RIP condition [23], then we can recover the considered scene $\mathbf{x}$ by solving the Lasso [40], a kind of L_1 regularization problem as

$$\hat{\mathbf{x}} \;=\; \arg\min_{\mathbf{x}} \;\; \left\{\frac{1}{2}\left\|\mathbf{y}_d - \boldsymbol{\Phi}\mathbf{x}\right\|_2^2 \;+\; \zeta\|\mathbf{x}\|_1\right\} \tag{24}$$

where ζ is the regularization parameter. After above recovery, $\mathbf{x}$ should be reshaped back into a matrix representing the backscattering of 2-D considered scene.

The optimization problem $arg\min\limits_{\mathbf{x}}\left\{\frac{1}{2}\left\|\mathbf{v} - \mathbf{x}\right\|_2^2 + \zeta\|\mathbf{x}\|_1\right\}$ has a closed form solution

$$\beta\,(\mathbf{v};\zeta) \;\overset{\Delta}{=}\; (|\mathbf{v}| - \zeta) \cdot e^{j \cdot \mathrm{angle}(\mathbf{v})} \cdot \mathbf{1}\,(|\mathbf{v}| > \zeta) \tag{25}$$

where $\mathbf{1}\,(\cdot)$ is the indicator factor, $\mathrm{angle}\,(\cdot)$ indicates the phase of a complex number, and $\beta\,(\cdot;\zeta)$ is the complex soft thresholding function applied component-wise to the input element $\mathbf{v}$.

C. *CAMP Iterative Algorithm*

L_1 regularization problem can be solved efficiently by several algorithms, *e.g.*, ITA. However, in SAR imaging, these existing algorithms will not obtain an image that preserves the background statistical properties as MF result, which restrict the further application of the regularization reconstruction SAR image, *e.g.*, CFAR detection. CAMP introduces a "state evolution" (SE) term which represents the evolution of the "noise" standard deviation as the iteration proceeds, and produces sparse and non-sparse (noisy) estimations of considered scene at the same time [36]. Thus, not only can we obtain a sparse solution of the considered scene as other regularization recovery algorithms, but also a non-sparse image with similar background distribution as MF recovered result. The CAMP iterative recovery algorithm used to solve the L_1 regularization problem (24) is detailed in Table I, where μ is the iterative parameter, σ_t is the standard deviation of the "noise" vector,

$$\mathbf{z}^{(t)} \;\overset{\Delta}{=}\; \tilde{\mathbf{x}}^{(t)} \;-\; \mathbf{x} \tag{26}$$

with $\tilde{\mathbf{x}}^{(t)}$ being the non-sparse estimation of the considered scene $\mathbf{x}$ at tth iteration. $\left|\tilde{\mathbf{x}}^{(t+1)}\right|_{k+1}$ denotes the $k+1$ largest component of $\left|\tilde{\mathbf{x}}^{(t+1)}\right|$ with $k = \|\mathbf{x}\|_0$. δ is the down-sampling ratio with $\delta = L/N$, $\langle\cdot\rangle$ is the average operator, β^R and β^I are the real and imagery part of complex soft thresholding function, β, and $\frac{\partial\beta^R}{\partial x_R}$ and $\frac{\partial\beta^I}{\partial x_I}$ are the partial derivative of β^R and β^I with respect to the real and imagery part of input element, respectively.

TABLE I

CAMP ALGORITHM FOR L_1 REGULARIZATION BASED TOPS SAR IMAGING

```
Input:-      Down-sampled echo data $\mathbf{y}_d$, Measurement matrix $\mathbf{\Phi}$
Initial:     $\hat{\mathbf{x}}^{(0)} = \mathbf{0}$, $\mathbf{w}^{(0)} = \mathbf{y}_d$
             Iterative parameter $\mu$, Error parameter $\varepsilon$, Maximum iterative step $T_{\max}$
Iteration:   While $t \leq T_{\max}$ and Residual $> \varepsilon$
  Step1:         $\tilde{\mathbf{x}}^{(t+1)} = \mathbf{\Phi}^{\mathrm{H}} \mathbf{w}^{(t)} + \hat{\mathbf{x}}^{(t)}$
  Step2:         $\sigma_{t+1} = \left| \tilde{\mathbf{x}}^{(t+1)} \right|_{k+1}$
  Step3:         $\mathbf{w}^{(t+1)} = \mathbf{y} - \mathbf{\Phi} \hat{\mathbf{x}}^{(t)} + \mathbf{w}^{(t)} \frac{1}{2\delta} \left( \left\langle \frac{\partial \beta^R}{\partial x_R} \left( \tilde{\mathbf{x}}^{(t+1)}; \mu\sigma_{t+1} \right) \right\rangle + \left\langle \frac{\partial \beta^I}{\partial x_I} \left( \tilde{\mathbf{x}}^{(t+1)}; \mu\sigma_{t+1} \right) \right\rangle \right)$
  Step4:         $\hat{\mathbf{x}}^{(t+1)} = \beta \left( \tilde{\mathbf{x}}^{(t+1)}; \mu\sigma_{t+1} \right)$
  Step5:         Residual $= \left\| \hat{\mathbf{x}}^{(t+1)} - \hat{\mathbf{x}}^{(t)} \right\|_2$
  Step6:         $t = t + 1$
             end
Output:      Reconstructed sparse image $\hat{\mathbf{x}} = \hat{\mathbf{x}}^{(t+1)}$
             Reconstructed non-sparse image $\tilde{\mathbf{x}} = \tilde{\mathbf{x}}^{(t+1)}$
```

IV. ECS-BAS BASED AZIMUTH-RANGE DECOUPLE L_1 REGULARIZATION TOPS SAR IMAGING VIA CAMP (L1-ECS-BAS-CAMP)

In this section, using ECS-BAS algorithm depicted in Section II as the imaging operator $\mathcal{R}(\cdot)$, we propose and derive a CAMP based azimuth-range decouple L_1 regularization TOPS SAR focusing mechanism, and demonstrate it from model construction, iterative recovery, parameter setting, to computational cost analysis in detail.

A. Model

Similar to 1-D imaging in Section III, we can write the 2-D TOPS SAR imaging model without down-sampling as

$$\mathbf{Y} = \mathbf{A}\mathbf{X} \tag{27}$$

where $\mathbf{Y} \in \mathbb{C}^{N_\eta \times N_\tau}$ is the 2-D echo data; $\mathbf{X} \in \mathbb{C}^{N_P \times N_Q}$ is the backscattered coefficient of the surveillance region; and $\mathbf{A}$ is the TOPS SAR radar system observation matrix constructed based on (1) and TOPS imaging geometry. After performing down-sampling of $\mathbf{Y}$, and considering the existing of noise $\mathbf{N}_0$, down-sampled 2-D echo data $\mathbf{Y}_d$ can be expressed as

$$\mathbf{Y}_d = \mathbf{\Xi} \circ \mathbf{Y} = \mathbf{\Xi} \circ (\mathbf{A}\mathbf{X}) + \mathbf{N_0} \tag{28}$$

where operation $\circ$ is the Hadamard product, $\mathbf{\Xi} \in \mathbb{R}^{N_\eta \times N_\tau}$ is the binary down-sampling matrix, which represents the sparse sampling strategy of $\mathbf{Y}$.

B. Principle of L1-ECS-BAS-CAMP

According to the model in (28), we can achieve the L_1 regularization reconstruction of considered scene by solving the optimization problem

$$\hat{\mathbf{X}} = \arg\min_{\mathbf{X}} \left\{ \frac{1}{2} \| \mathbf{Y}_d - \mathbf{\Xi} \circ (\mathbf{A}\mathbf{X}) \|_F^2 + \gamma \| \mathbf{X} \|_1 \right\} \tag{29}$$

where $\hat{\mathbf{X}}$ is the L_1 regularization recovered backscattered coefficient of 2-D considered scene, $\|\cdot\|_F$ is the Frobenius norm of a matrix, and γ is the regularization parameter.

It should be noted that, since TOPS SAR imaging observation matrix $\mathbf{A}$ could not be constructed directly based on the relationship between 2-D echo data $\mathbf{Y}$ and backscattered coefficient $\mathbf{X}$, thus we can not achieve the regularization reconstruction of considered scene by solving the optimization problem (29). An alterative method is introduced in Section III. However, its computational cost is unacceptable in the practical processing of huge raw data. Therefore, if we want to use regularization technique to recover the large-scale surveillance region, azimuth-range decouple is essential so as to reduce the computational complexity and memory occupation efficiently.

In TOPS, conventional MF based imaging procedure $\mathcal{R}(\cdot)$, *e.g.*, ECS-BAS introduced in Section II, can be expressed as

$$\mathbf{X}_{MF} = \mathcal{R}(\mathbf{Y}). \tag{30}$$

After introducing the exact observation model (27) to (30), the relationship between backscattered coefficient of considered scene $\mathbf{X}$ and MF recovered image $\mathbf{X}_{MF}$ can be written as

$$\mathbf{X}_{MF} \;=\; \mathcal{R}\left(\mathbf{Y}\right) \;=\; \mathcal{R}\left(\mathbf{A}\mathbf{X}\right). \tag{31}$$

It is known that $\mathbf{X}_{MF}$ is always the approximation of $\mathbf{X}$ because of the existing of artifacts, *e.g.*, sidelobes, noise. Therefore, for the relationship shown in (31), if $\mathcal{R}\mathbf{A} \approx \mathbf{I}$, then we can use the inverse of $\mathcal{R}$, *i.e.*, $\mathcal{R}^{-1}$ to approximate $\mathbf{A}$. Based on this, the basic idea of azimuth-range decouple is replacing the radar observation matrix $\mathbf{A}$ with an approximated observation operator, or called echo simulation operator, which performs the transformation from complex reflectivity image to original echo data, This principle can be generalized as

$$\mathcal{M}\left(\mathbf{X}\right) \;=\; \mathcal{R}^{-1}\left(\mathbf{X}\right) \;\approx\; \mathbf{A}\mathbf{X} \tag{32}$$

with $\mathcal{M}\left(\cdot\right)$ being the echo simulation operator, which is an approximation of radar observation matrix $\mathbf{A}$.

After above replacement, we can rewrite the optimization problem in (29) of L_1 regularization TOPS SAR imaging as

$$\hat{\mathbf{X}} \;=\; \min_{\mathbf{X}} \left\{ \frac{1}{2}\left\|\mathbf{Y}_d \;-\; \Xi_a \circ \mathcal{M}\left(\mathbf{X}\right) \circ \Xi_r\right\|_F^2 \;+\; \gamma\left\|\mathbf{X}\right\|_1 \right\} \tag{33}$$

where $\Xi_a \in \mathbb{R}^{N_r \times N_\tau}$ and $\Xi_\tau \in \mathbb{R}^{N_\eta \times N_\tau}$ are the binary matrix which denote the down-sampling strategy in azimuth and range directions, respectively.

C. Iterative Recovery of L1-ECS-BAS-CAMP

As shown in Fig. 2, the ECS-BAS TOPS SAR imaging procedure $\mathcal{R}\left(\cdot\right)$ can be expressed as

$$\begin{aligned}\mathcal{R}\left(\mathbf{Y}\right) \;=\; & \mathbf{F}_a^{-1}\left(\mathbf{F}_a\boldsymbol{\Gamma}_{sum}\left[\mathbf{F}_a^{-1}\left(\mathbf{F}_a\boldsymbol{\Gamma}_{sub}\left[\mathbf{Y}\right] \circ \boldsymbol{\Theta}_1\mathbf{F}_r\right.\right.\right. \\ & \left.\left.\left.\circ\; \boldsymbol{\Theta}_2\mathbf{F}_r^{-1} \circ \boldsymbol{\Theta}_3 \circ \boldsymbol{\Theta}_4\right) \circ \boldsymbol{\Theta}_5\right] \circ \boldsymbol{\Theta}_6\right).\end{aligned} \tag{34}$$

As above discussion, we know that echo simulation operator $\mathcal{M}\left(\cdot\right)$ is the inverse of $\mathcal{R}\left(\cdot\right)$. Thus, according to the procedure shown in (34), we can write $\mathcal{M}\left(\cdot\right)$ as (see Fig. 2)

$$\begin{aligned}\mathcal{M}\left(\mathbf{X}\right) \;=\; & \boldsymbol{\Gamma}_{sub}\left[\mathbf{F}_a^{-1}\left(\mathbf{F}_a\boldsymbol{\Gamma}_{sum}\left[\mathbf{F}_a^{-1}\left(\mathbf{F}_a\mathbf{X} \circ \boldsymbol{\Theta}_6^{\mathrm{H}}\right) \circ \boldsymbol{\Theta}_5^{\mathrm{H}}\right]\right.\right. \\ & \left.\left.\circ\; \boldsymbol{\Theta}_4^{\mathrm{H}} \circ \boldsymbol{\Theta}_3^{\mathrm{H}}\mathbf{F}_r \circ \boldsymbol{\Theta}_2^{\mathrm{H}}\mathbf{F}_r^{-1} \circ \boldsymbol{\Theta}_1^{\mathrm{H}}\right)\right]\end{aligned} \tag{35}$$

where symbol $\left(\cdot\right)^{\mathrm{H}}$ is the conjugate transpose operation. Due to $\mathcal{R}\left(\cdot\right)$ and $\mathcal{M}\left(\cdot\right)$ in (34) and (35) are reversible operators for each other, thus for the considered scene $\mathbf{X}$, we have

$$\mathbf{X} \;=\; \mathcal{R}\left(\mathcal{M}\left(\mathbf{X}\right)\right). \tag{36}$$

Similar to 1-D reconstruction shown in Table I, in the following, we will derive the 2-D matrix operation based CAMP iterative recovery algorithm to solve the optimization problem (33). Firstly, we initialize the reconstructed sparse and non-sparse estimations of considered scene as $\hat{\mathbf{X}}^{(0)} = \mathbf{0}$ and $\tilde{\mathbf{X}}^{(0)} = \mathbf{0}$, respectively; and the echo data matrix as $\mathbf{W}^{(0)} = \mathbf{Y}_d$. For tth step, non-sparse image is estimated as

$$\tilde{\mathbf{X}}^{(t+1)} \;=\; \mathcal{R}\left(\Xi_a^{\mathrm{T}} \circ \mathbf{W}^{(t)} \circ \Xi_r^{\mathrm{T}}\right) \;+\; \hat{\mathbf{X}}^{(t)}. \tag{37}$$

After adaptively setting σ_{t+1} as $\sigma_{t+1} = \left|\tilde{\mathbf{X}}^{(t+1)}\right|_{k+1}$, we will update the echo data by using

$$\begin{aligned}\mathbf{W}^{(t+1)} \;=\; & \mathbf{Y}_d \;-\; \Xi_a \circ \mathcal{M}\left(\hat{\mathbf{X}}^{(t)}\right) \circ \Xi_r \;+\; \mathbf{W}^{(t)}\frac{1}{2\delta} \\ & \cdot\; \left(\left\langle \frac{\partial \beta^R}{\partial x_R}\left(\tilde{\mathbf{X}}^{(t+1)}; \mu\sigma_{t+1}\right)\right\rangle\right. \\ & \left.+\; \left\langle \frac{\partial \beta^I}{\partial x_I}\left(\tilde{\mathbf{X}}^{(t+1)}; \mu\sigma_{t+1}\right)\right\rangle\right)\end{aligned} \tag{38}$$

and then recover the sparse image $\hat{\mathbf{X}}^{(t+1)}$ by means of

$$\hat{\mathbf{X}}^{(t+1)} \;=\; \beta\left(\tilde{\mathbf{X}}^{(t+1)}; \mu\sigma_{t+1}\right). \tag{39}$$

If condition $\left\|\hat{\mathbf{X}}^{(t+1)} - \hat{\mathbf{X}}^{(t)}\right\|_F \Big/ \left\|\hat{\mathbf{X}}^{(t)}\right\|_F \leqslant \varepsilon$ or $t = T_{max}$ satisfies, with ε being a constant error parameter, above iteration will be stopped, and outputs the final reconstructed sparse and non-sparse images of considered scene as

$$\begin{aligned}\hat{\mathbf{X}} \;&=\; \hat{\mathbf{X}}^{(t+1)} \\ \tilde{\mathbf{X}} \;&=\; \tilde{\mathbf{X}}^{(t+1)}.\end{aligned} \tag{40}$$

Otherwise, let $t = t + 1$, the iteration will be continued.

After above regularization recovery, operation matrix $\boldsymbol{\Theta}_7$ will be used to perform phase compensation as

$$\begin{aligned}\hat{\mathbf{X}} \;&=\; \hat{\mathbf{X}} \;\circ\; \boldsymbol{\Theta}_7 \\ \tilde{\mathbf{X}} \;&=\; \tilde{\mathbf{X}} \;\circ\; \boldsymbol{\Theta}_7.\end{aligned} \tag{41}$$

D. Parameter Employed

The meaning of several components in the proposed L1-ECS-BAS-CAMP method are shown as following.

1) The "noise" matrix, $\mathbf{Z}^{(t)}$ is defined as

$$\mathbf{Z}^{(t)} \;\triangleq\; \tilde{\mathbf{X}}^{(t)} \;-\; \mathbf{X}. \tag{42}$$

2) σ_t is the standard deviation of $\mathbf{Z}^{(t)}$, and $\sigma_* = \lim\limits_{t\to\infty} \sigma_t$. In practical TOPS SAR imaging, the noise and clutter distributions are unknown, so we use $\sigma_t = \left|\tilde{\mathbf{X}}^{(t)}\right|_{k+1}$ as an estimation of σ_t in this paper.

3) Regularization parameter, γ, should be chosen to satisfy

$$0 \;<\; \gamma \;\leq\; \left\|\mathbf{X}_{MF}\right\|_1 \tag{43}$$

where $\mathbf{X}_{MF}$ is the recovered image of MF based TOPS SAR imaging algorithm.

4) The set of iterative parameter μ relies on σ_* and γ. CAMP algorithm and Lasso problem are connected through the relationship between μ and γ. According to the analysis in [36], if μ satisfies

$$\begin{aligned}\gamma \triangleq\ & \mu\sigma_*\left(1-\frac{1}{2\delta}\mathbb{E}\left(\left\langle\frac{\partial\beta^R}{\partial x_R}\left(\mathbf{X}_{MF};\mu\sigma_*\right)\right\rangle\right.\right.\\ &+\left.\left.\left\langle\frac{\partial\beta^I}{\partial x_I}\left(\mathbf{X}_{MF};\mu\sigma_*\right)\right\rangle\right)\right) \qquad (44)\end{aligned}$$

then CAMP with iterative parameter μ can be used to solve the Lasso problem with regularization parameter γ. Where $\mathbb{E}(\cdot)$ is the expectation operator. In L1-ECS-BAS-CAMP, we set $\sigma_* = |\mathbf{X}_{MF}|_{k+1}$, and $\gamma_{\max}=\|\mathbf{X}_{MF}\|_1$, to estimate the upper bound of μ as $\mu_{\max}$ through (44).

E. Computational Cost

Let I denote the required iterative steps of accurate recovery, $M = N_\eta \times N_\tau$ and $N = N_P \times N_Q$. Then the computational complexity of conventional ECS-BAS algorithm is $C_{ECS-BAS} = \mathcal{O}(M\log(M))$. For each iteration of the proposed method, its computation includes two main parts, the calculations of an inverse ECS-BAS and a ECS-BAS procedure, which has complexity of $\mathcal{O}(M\log(M))$, and a decouple thresholding operation with complexity $\mathcal{O}(N)$. Thus the total computational complexity of L1-ECS-BAS-CAMP is of the order $C_{Pro} = \mathcal{O}(IM\log(M))$. For conventional L_1 regularization method, as discussed in Section III, it needs to transfer the 2-D echo data into a vector and reconstruct the considered scene via 2-D matrix operations for every image point in turn, which complexity reaches $C_{L1} = \mathcal{O}(IMN)$. This is unacceptable for large-scale TOPS SAR imaging. Compared to conventional L_1 regularization approach, the accelerated rate of the proposed method is approximately

$$r_C = \frac{C_{L1}}{C_{Pro}} = \mathcal{O}\left(\frac{N}{\log(M)}\right). \qquad (45)$$

In memory occupation, since L1-ECS-BAS-CAMP only needs to storage the input, output and several matrices shown in Fig. 2, its memory requirement is only around $M_{Pro} = \mathcal{O}(N)$ bytes which at the same order as ECS-BAS. In comparison, since conventional L_1 regularization method performs the sparse reconstruction based on a measurement matrix which size is $M \times N$, and hence its memory occupation is extremely large, approximately $M_{L1} = \mathcal{O}(MN)$ bytes.

Above analysis shows that compared to conventional L_1 regularization approach, the proposed method reduces the computational complexity and memory occupation to the same order as ECS-BAS based TOPS SAR imaging algorithm, and hence makes regularization reconstruction of large-scale considered scene in TOPS become possible.

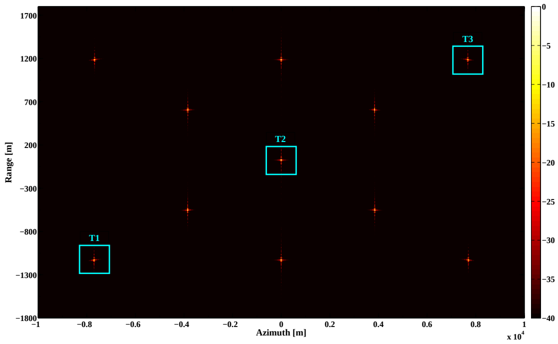

Fig. 3. Surveillance region in the simulation (in dB).

TABLE II
SIMULATION PARAMETERS

Parameter	Value
Carrier frequency	9.65 GHz
Azimuth beamwidth (3 dB)	0.36°
Platform effective velocity	7200.00 m/s
Platform height	500.00 km
Mean lookangle	30.00°
System PRF	3456.00 Hz
Antenna length	5.00 m
Azimuth beam rotation rate	$5.00^{\circ}/s$
Burst duration	0.40 s
Transmitted pulse duration	5.00 μs
Transmitted pulse bandwidth	15.00 MHz
Sampling frequency	20.00 MHz

V. EXPERIMENTAL RESULT AND DISCUSSION VIA SIMULATED DATA

In this section, we perform several experiments based on the simulated data along with a discussion to validate the proposed method. As shown in Fig. 3, ten point targets located on the different positions are set as surveillance region. The size of surveillance region is (3890 m (Range) × 23080 m (Azimuth)). Simulation parameters are listed in Table II. All experiments will be conducted on a workstation of 8-core 2.20-GHz Inter Core i5-5200U CPU with 16 GB memory. The algorithms are implemented in Matlab 2013a. Since the restriction of memory requirement and computational time, in the experiments, we only use the ECS-BAS recovered images as comparison to illustrate the validity of L1-ECS-BAS-CAMP in the image performance improvement. To demonstrate the experimental results intuitively and clearly, three point targets, called T1, T2, and T3 (see Fig. 3), are chosen as the example to validate L1-ECS-BAS-CAMP. The relative location (reference is the center of surveillance region) of T1, T2, and T3 are (-1125 m (Range) × -7700 m (Azimuth)), (0 m (Range) × 0 m (Azimuth)), and (1125 m (Range) × 7700 m (Azimuth)).

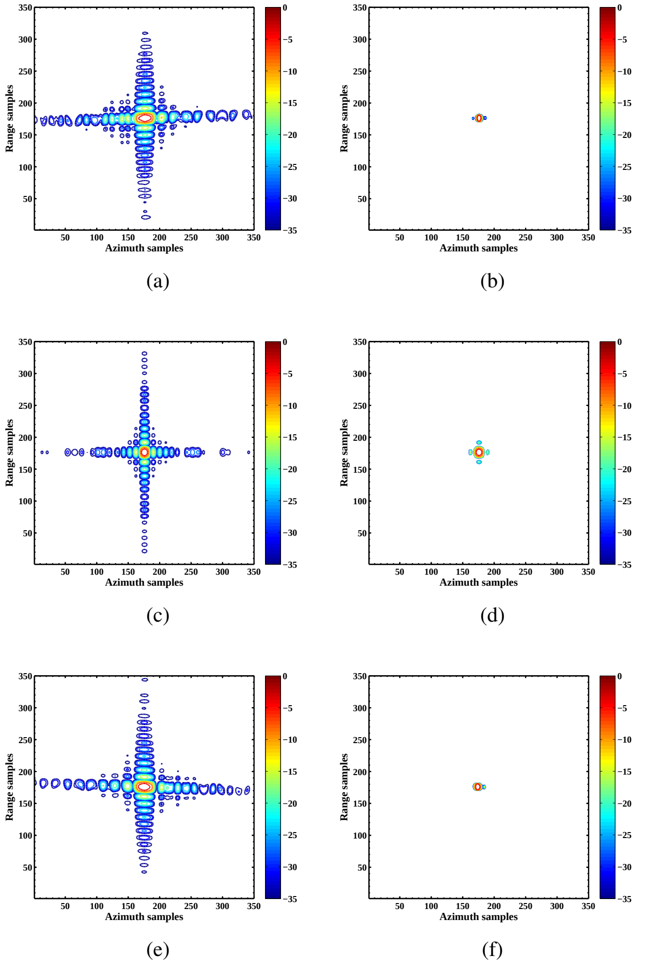

(a) (b)

(c) (d)

(e) (f)

Fig. 4. Contour plots of three point targets (in dB). (a) T1 (ECS-BAS). (b) T1 (L1-ECS-BAS-CAMP (Sparse image)). (c) T2 (ECS-BAS). (d) T2 (L1-ECS-BAS-CAMP (Sparse image)). (e) T3 (ECS-BAS). (f) T3 (L1-ECS-BAS-CAMP (Sparse image)).

A. Sidelobe Suppression

Fig. 4 is the contour plots of T1, T2, and T3 reconstructed by ECS-BAS (Left column) and the proposed L1-ECS-BAS-CAMP (sparse image) (Right column) algorithms, respectively. In order to validate the effect of sidelobe suppression of L1-ECS-BAS-CAMP clearly, we didn't add any noise and clutter to the simulated echo data of point targets. Fig. 4 shows that both methods can recover three point targets accurately, while L1-ECS-BAS-CAMP can reduce sidelobes efficiently, regardless of azimuth or range direction, even remove sidelobes completely (range direction in Fig. 4(f)). However, it should be noted that these results were obtained in an ideal condition, *i.e.*, signal to clutter and noise ratio $\mathrm{SCNR} = \infty$. In practical TOPS SAR imaging, we could not expect to achieve such perfect suppression.

B. Noise and Clutter Suppression

In this simulation, to perform meaningful comparisons, we artificially introduced some noise and clutter to the simulated echo data of surveillance region. Real part of the simulated TOPS SAR echo data before and after adding noise and clutter is shown in Fig. 5. Fig. 6 is the contour plots of three selected point targets recovered by ECS-BAS (Left column) and L1-ECS-BAS-CAMP (sparse image) (Right column) via the echo data with noise and clutter. Compared to ECS-BAS, we can see that the proposed method suppresses noise and clutter efficiently and recovers the position of all point targets accurately. To evaluate the noise and clutter suppression ability of L1-ECS-BAS-CAMP quantitatively, we introduce

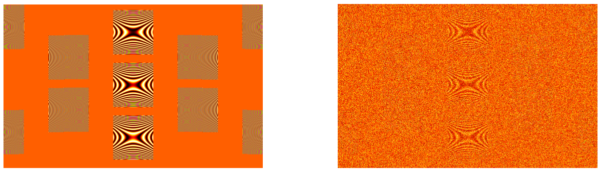

(a) (b)

Fig. 5. Real part of the simulated echo data (a) before and (b) after adding noise and clutter.

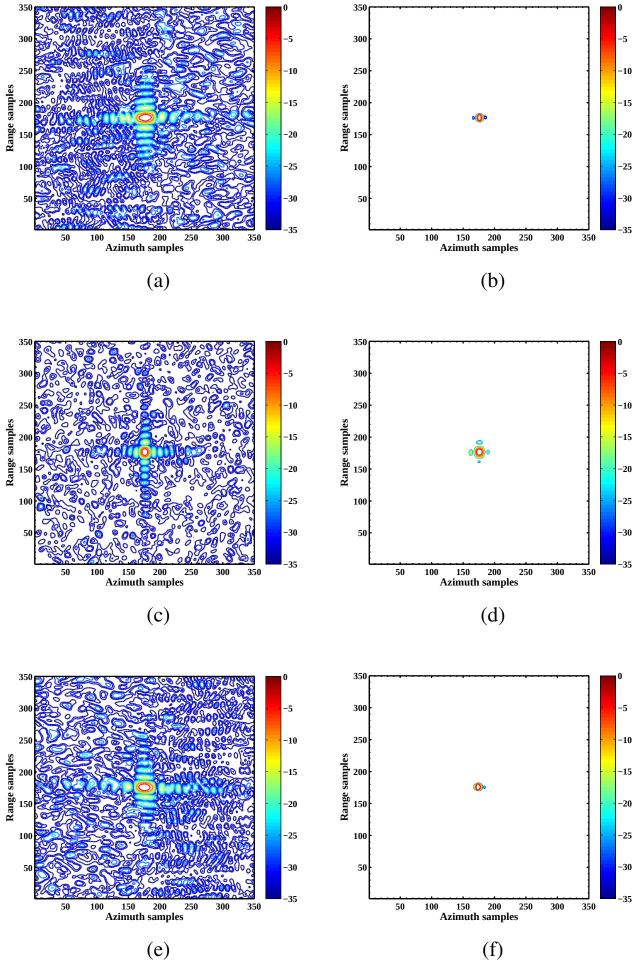

(a) (b)

(c) (d)

(e) (f)

Fig. 6. Contour plots of point targets based on the simulated echo data with noise and clutter (in dB). (a) T1 (ECS-BAS). (b) T1 (L1-ECS-BAS-CAMP (Sparse image)). (c) T2 (ECS-BAS). (d) T2 (L1-ECS-BAS-CAMP (Sparse image)). (e) T3 (ECS-BAS). (f) T3 (L1-ECS-BAS-CAMP (Sparse image)).

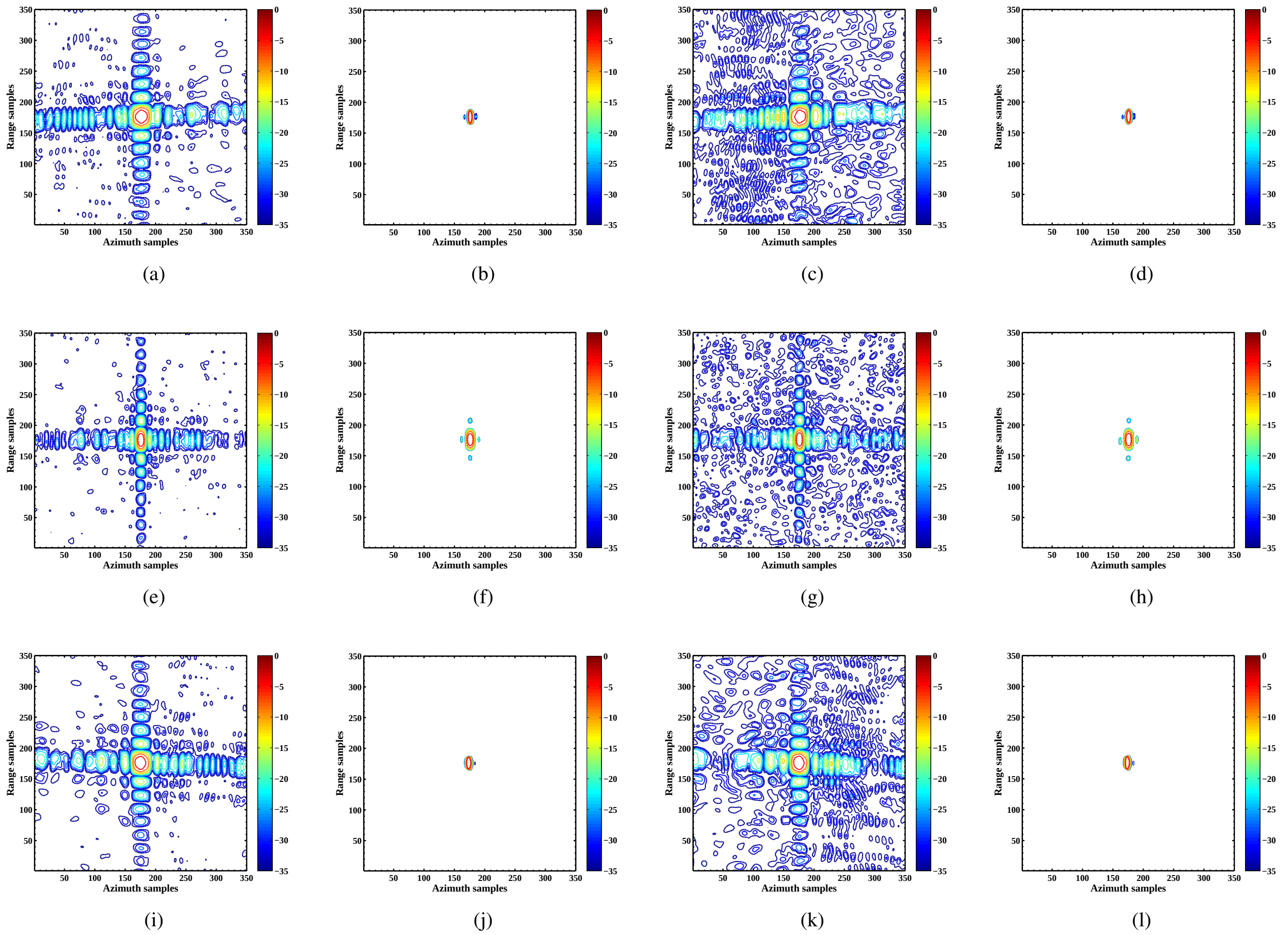

(a) (b) (c) (d)

(e) (f) (g) (h)

(i) (j) (k) (l)

Fig. 7. Contour plots of three point targets based on 50% and 25% random down-sampled simulated echo data (in dB). From left to right: ECS-BAS with 50% echo data, L1-ECS-BAS-CAMP with 50% echo data, ECS-BAS with 25% echo data, L1-ECS-BAS-CAMP with 25% echo data. (Upper row) T1. (Middle row) T2. (Lower row) T3.

the target-to-background ratio (TBR) [41]

$$\mathrm{TBR}\left(\mathbf{X}\right) \triangleq 20\log_{10}\left(\frac{\max_{(p,q)\in\mathcal{T}}\left|\left(\mathbf{X}\right)_{(p,q)}\right|}{\left(1/N_{\mathcal{B}}\right)\sum_{(p,q)\in\mathcal{B}}\left|\left(\mathbf{X}\right)_{(p,q)}\right|}\right) \tag{46}$$

where $\mathcal{T}$ indicates the target area, which is surrounded by the background region, $\mathcal{B}$ whose number of pixels is $N_{\mathcal{B}}$. Quantitative analysis of noise and clutter suppression with TBR is shown in Table III. Its result accords with the visual representation in Fig. 6, *i.e.*, L1-ECS-BAS-CAMP significantly outclasses ECS-BAS in noise and clutter suppression, and reduces TBR approximately 40 dB, which means that nearly all noise and clutter are removed.

C. Down-sampling Recovery

An advantage of CS is that it can recover the original sparse signal from far less samples than the sampling theory requires. Thus, in practical data collection of SAR system, we can achieve larger swath by reducing the number of sampling points. To demonstrate the validity of our proposed algorithm in down-sampled echo data based TOPS SAR imaging, we perform 50% and 25% random down-sampling for full-sampled echo data shown in Fig. 5(a), and reconstruct the considered scene by ECS-BAS and L1-ECS-BAS-CAMP, respectively (see Fig. 7). Fig. 7 depicts that since the lack of samples, ECS-BAS could not recover the point targets successfully with obvious ambiguities and energy dispersion. While L1-ECS-BAS-CAMP also can reconstruct the considered scene well with lower sidelobes even only using 25% samples.

TABLE III
TBR IN THE IMAGES RECONSTRUCTED BY DIFFERENT METHODS

Target	**Target 1**	**Target 2**	**Target 3**
ECS-BAS	30.16 dB	30.55 dB	30.85 dB
L1-ECS-BAS-CAMP	70.38 dB	67.86 dB	68.85 dB

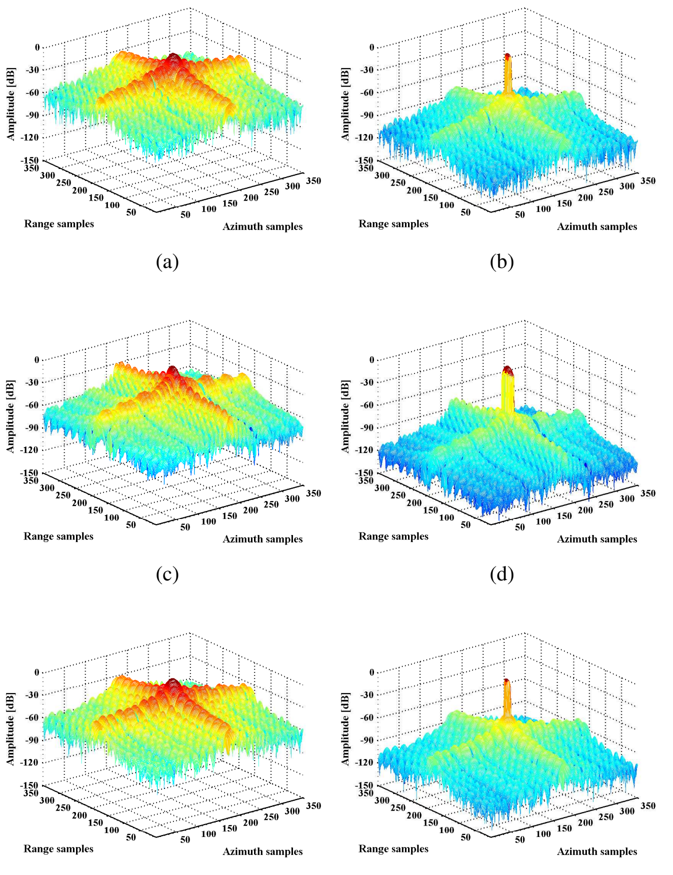

(a) (b)

(c) (d)

(e) (f)

Fig. 8. Normalized reconstructed images of three point targets (in dB). (a) T1 (ECS-BAS). (b) T1 (L1-ECS-BAS-CAMP (Non-sparse image)). (c) T2 (ECS-BAS). (d) T2 (L1-ECS-BAS-CAMP (Non-sparse image)). (e) T3 (ECS-BAS). (f) T3 (L1-ECS-BAS-CAMP (Non-sparse image)).

D. Non-sparse Reconstruction of Surveillance Region

As above discussion of CAMP in Section III and Section IV, compared to other L_1 regularization recovery algorithms, the superiority of CAMP is that it can obtain both sparse and non-sparse estimations simultaneously of original signal. In above simulations, to validate the effectiveness of the proposed method in performance improvement, the sparse images recovered by L1-ECS-BAS-CAMP are enough. In this experiment, Fig. 8 shows the reconstructed non-sparse image of three point targets (Right column) by the proposed method along with the results of ECS-BAS (Left column) based on the simulated echo data shown in Fig. 5(a). Note that the non-sparse images not only protrude the target as recovered sparse images, but also retain the background distribution as ECS-BAS results only with amplitude decreased approximately 50 dB. This characteristic will be very helpful in CFAR [37].

E. Dependence on Iterative Parameter μ

In the proposed method, μ is a parameter controls the convergence speed of iterative algorithm, which should satisfy

$$0 < \mu_{max}^{-1} \leq \mu^{-1} \leq 1. \tag{47}$$

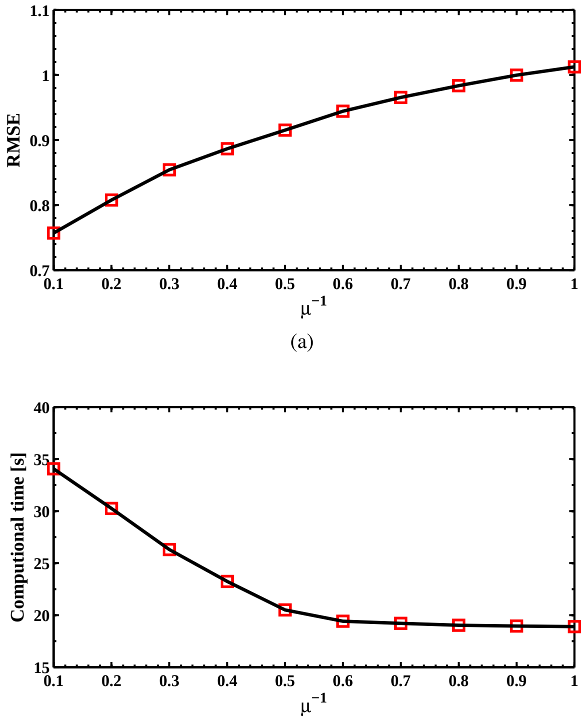

(a)

(b)

Fig. 9. (a) Recovered precision based on RMSE, and (b) computational time of the proposed method as a function of iterative parameter μ^{-1}.

When μ^{-1} moves from 0 to 1, the convergence speed of L1-ECS-BAS-CAMP will increase, while the precision of recovered solution will decrease. In the experiments of this subsection, using MF recovered image $\mathbf{X}_{MF}$ of considered scene shown in Fig. 3, we can calculate the maximum value of γ as $\gamma_{max} = \|\mathbf{X}_{MF}\|_1 = 35.45$, and then estimate the upper bound of μ based on the relationship in (44) as $\mu_{max}^{-1} \approx 0.05$. To give an impression about the impact of iterative parameter μ on the performance of the proposed method, Fig. 9 shows the recovered precision and convergence speed of L1-ECS-BAS-CAMP as a function of μ^{-1}. In Fig. 9(a), we use relative mean square error (RMSE) as the judging criterion of recovered precision. It says that the reconstructed accuracy of L1-ECS-BAS-CAMP is inversely proportional to the value of μ^{-1}. While the computational time will decrease when μ^{-1} moves from 0 to 1 (see Fig. 9(b)). This experimental result accords with above theoretical analysis. Based on this, in practical TOPS SAR imaging, the value of μ should be selected as a compromise between convergence speed and recovered precision. In this paper, after considering above two factors, we set $\mu^{-1} = 0.5$.

VI. PERFORMANCE ANALYSIS

In above theoretical analysis, we know that a main advantage of L1-ECS-BAS-CAMP is less computational time and lower memory requirement compared with conventional L_1 regularization based TOPS SAR imaging method, and at the same order of ECS-BAS algorithm. While it also can achieve similar performance improvement of SAR images as L_1 regularization technique shown in Table I. In section V,

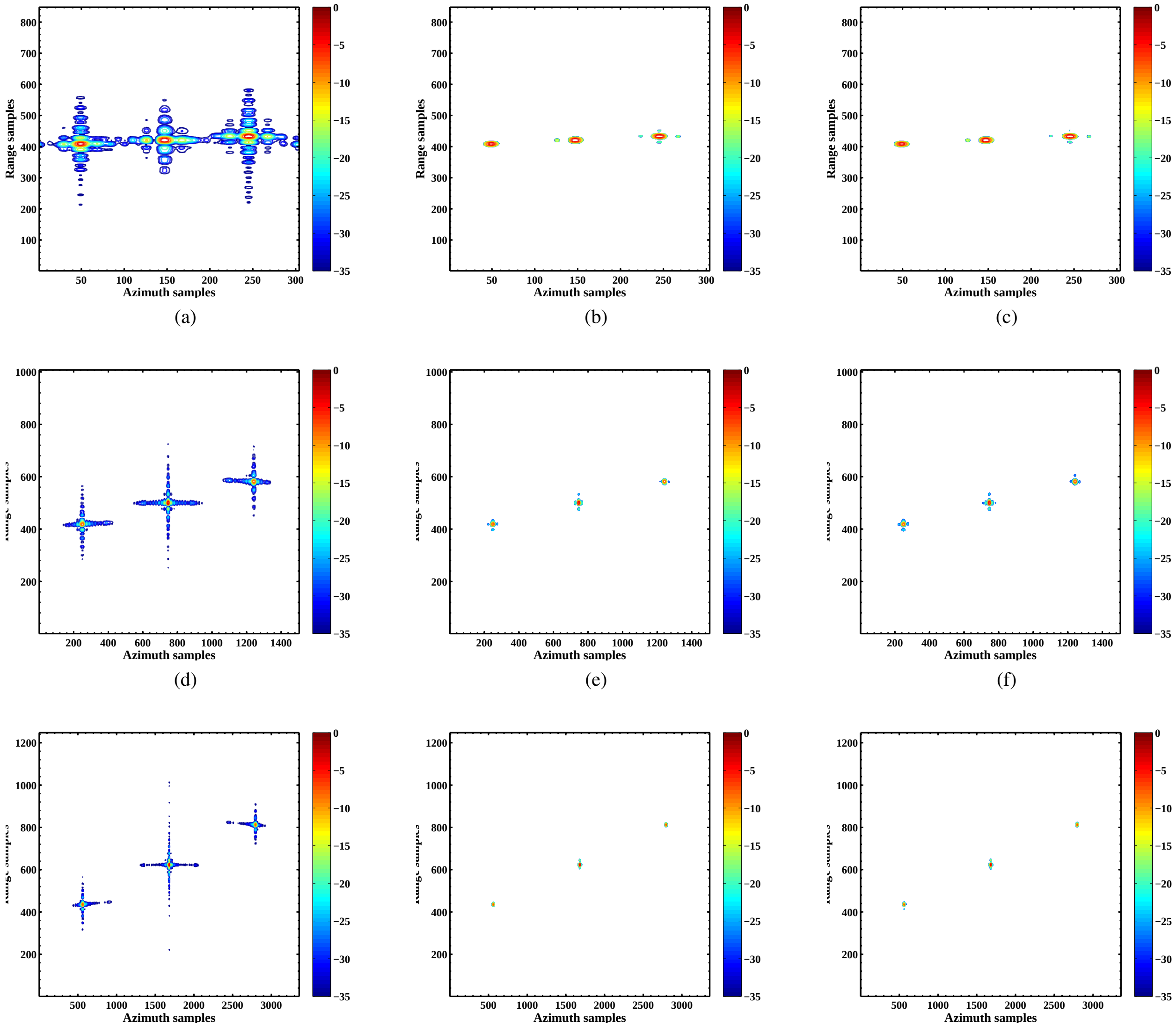

(a) (b) (c) (d) (e) (f) (g) (h) (i)

Fig. 10. Normalized reconstructed images of simulated point targets (in dB) by (Left column) ECS-BAS, (Middle column) L1-CAMP (Non-sparse image), and (Right colum) L1-ECS-BAS-CAMP (Non-sparse image), respectively. The size of considered scene is (Upper row) 38 (Range) × 106 (Azimuth) samples (304 × 848 after interpolation), (Middle row) 126 (Range) × 188 (Azimuth) samples (1008 × 1504 after interpolation), (Lower row) 156 (Range) × 420 (Azimuth) samples (1248 × 3340 after interpolation).

we have validated the effectiveness of the proposed method in image performance improvement and down-sampling imaging. In this section, to quantitatively evaluate the proposed method especially in the decrease of computational cost, we perform several experiments based on the smaller considered scenes, and obtain the images by not only ECS-BAS and the proposed L1-ECS-BAS-CAMP methods, but also the conventional L_1 regularization algorithm which has a higher requirement of computer performance. The simulation parameters are nearly identical to Table II except for the platform height H_r. In the experiments, we change the size of considered scene through setting different value of platform height. For clarity, the conventional CAMP based L_1 regularization TOPS SAR imaging method shown in Table I is denoted as L1-CAMP. It should be noted that the images shown in this paper are plotted after eight times interpolation of recovered results both in azimuth and range directions. In addition, all quantitative analysis are performed based on the non-sparse solutions of L1-CAMP and L1-ECS-BAS-CAMP in this section.

A. *Compare with L1-CAMP*

Fig. 10 shows the image reconstructed by ECS-BAS, along with the L1-CAMP and L1-ECS-BAS-CAMP recovered non-sparse estimations of considered scenes with different sizes by using full-sampled simulated echo data without any noise and clutter. From Fig. 10, we can see that no matter what size of considered scene is set, both L1-CAMP and L1-ECS-BAS-CAMP algorithms all can suppress sidelobes efficiently compared with MF based method, ECS-BAS, regardless of in azimuth or range direction. While L1-ECS-BAS-CAMP shows a similar ability in image performance improvement as conventional L_1 regularization TOPS SAR imaging technique.

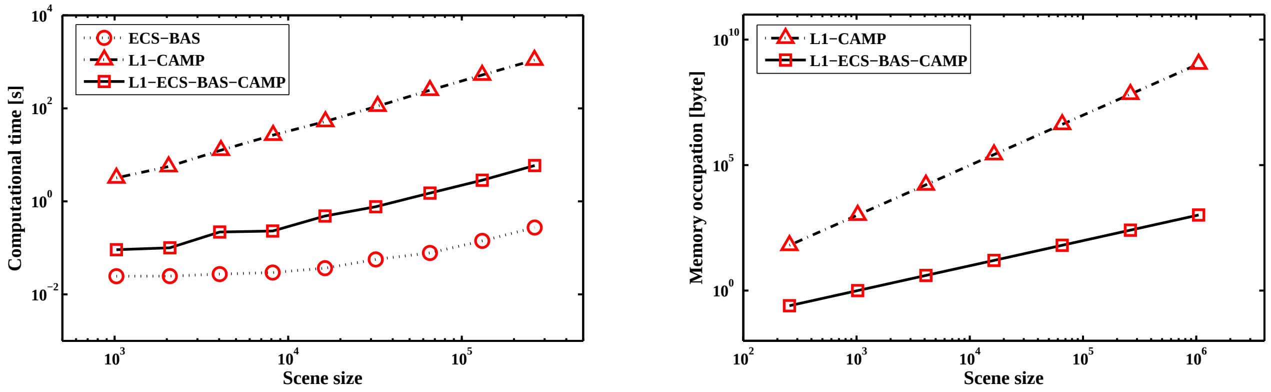

(a) (b)

Fig. 11. Computational cost of ECS-BAS, L1-CAMP, and L1-ECS-BAS-CAMP as a function of scene size. (a) Computational time. (b) Memory occupation.

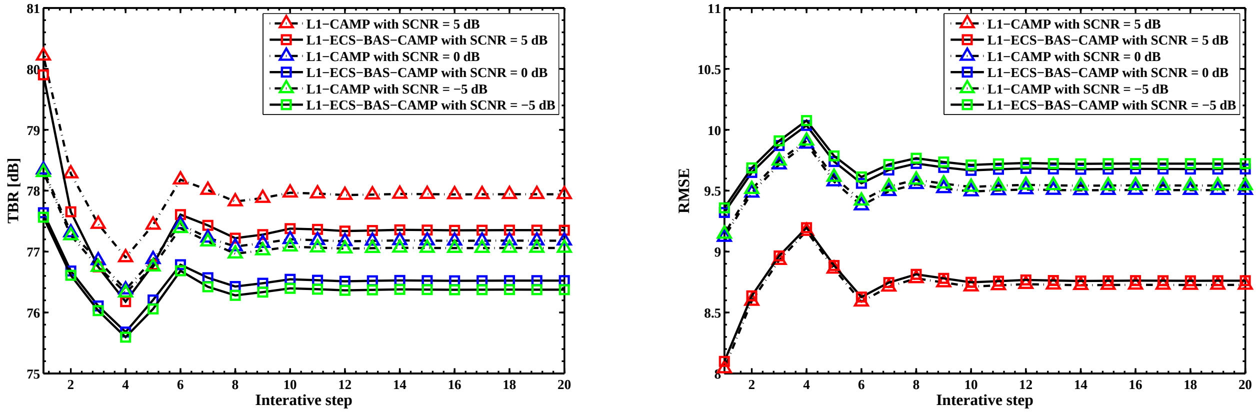

(a) (b)

Fig. 12. (a) TBR and (b) RMSE of the images reconstructed by L1-CAMP and L1-ECS-BAS-CAMP methods as a function of iterative step t.

B. Analysis of Computational Cost

Fig. 11 depicts the computational cost of ECS-BAS, L1-CAMP, and L1-ECS-BAS-CAMP methods under different sizes of considered scene. Fig. 11(a) shows that even if the scene size is just $242 \times 1086 \approx 2.62 \times 10^5$, we still need 10^3 seconds to recover the considered scene by using L1-CAMP algorithm. However, in practical SAR imaging including TOPS, the scene size is usually larger than 1024×8192, this means that L1-CAMP needs more than 12 days to achieve the regularization reconstruction of surveillance region with the working computer having at least 64 TB memory. This is unacceptable for the real-time processing. L1-ECS-BAS-CAMP relieves this pressure well, which reduces the computational time to the same order as MF algorithm (see Fig. 11(a)). Fig. 11(b) gives the memory requirement of L1-CAMP and L1-ECS-BAS-CAMP in TOPS SAR focusing. This result accords with above theoretical analysis, *i.e.*, the proposed method can reduce the memory occupation dramatically compared with L1-CAMP. In addition, we find that no matter for computed time or memory requirement, the difference between L1-CAMP and L1-ECS-BAS-CAMP will gradually enlarge as the scene size increases.

C. Recovery Accuracy and Convergence Speed Versus SCNR

In this subsection, we only set one point target located on the scene center as surveillance region whose size is 138 (Range) × 118 (Azimuth) samples, then artificially introduced some noise and clutter with $\mathrm{SCNR} = -5\ \mathrm{dB}, 0\ \mathrm{dB}, 5\ \mathrm{dB}$ to the simulated echo data, and reconstructed the considered scene by L1-CAMP and L1-ECS-BAS-CAMP via full-sampled echo data, respectively. The definition of SCNR is

$$\mathrm{SCNR} \triangleq 10 \log_{10} \left(\frac{P_t}{P_c} \right) \tag{48}$$

where P_t and P_c are the power of target and the power of noise and clutter, respectively.

Fig. 12 shows the TBR and RMSE of the recovered results as a function of iterative step t. We can see that no matter for TBR or RMSE, all curves of L1-CAMP and L1-ECS-BAS-CAMP with different SCNRs have a similar variation tendency, and will be converged to a fixed value after about 10 iterations. This convergent value is depended on the value of SCNR. It says that if less noise and

TABLE IV
PERFORMANCE OF THE RECONSTRUCTED IMAGES UNDER DIFFERENT COMBINATION OF SCNR AND DOWN-SAMPLING RATIO [dB]

SCNR = 10 dB	$\delta = 100\%$			$\delta = 50\%$			$\delta = 25\%$		
	TBR	**PSLR**	**ISLR**	**TBR**	**PSLR**	**ISLR**	**TBR**	**PSLR**	**ISLR**
ECS-BAS	57.01	-13.22	-09.67	43.86	-11.89	-06.03	39.12	-11.17	-03.43
L1-CAMP	80.15	-61.16	-57.03	79.58	-59.91	-53.51	78.28	-59.15	-50.79
L1-ECS-BAS-CAMP	79.73	-61.67	-57.66	78.48	-60.41	-54.12	77.36	-59.62	-51.43
SCNR = 0 dB	$\delta = 100\%$			$\delta = 50\%$			$\delta = 25\%$		
	TBR	**PSLR**	**ISLR**	**TBR**	**PSLR**	**ISLR**	**TBR**	**PSLR**	**ISLR**
ECS-BAS	43.31	-13.27	-09.34	38.05	-14.62	-07.04	34.24	-09.17	-03.01
L1-CAMP	79.47	-61.22	-56.70	77.91	-62.49	-54.28	76.62	-57.74	-50.48
L1-ECS-BAS-CAMP	78.35	-61.72	-57.32	76.92	-62.98	-54.92	75.86	-58.26	-51.15
SCNR = −10 dB	$\delta = 100\%$			$\delta = 50\%$			$\delta = 25\%$		
	TBR	**PSLR**	**ISLR**	**TBR**	**PSLR**	**ISLR**	**TBR**	**PSLR**	**ISLR**
ECS-BAS	24.78	-14.67	-01.73	20.43	-08.42	03.30	19.28	-08.26	03.76
L1-CAMP	70.60	-62.39	-48.62	67.57	-56.39	-44.07	66.64	-56.21	-43.52
L1-ECS-BAS-CAMP	70.46	-62.87	-49.26	67.47	-56.72	-44.53	66.67	-56.45	-43.85

clutter are added to the simulated echo data, higher TBR and lower RMSE, *i.e.*, a better image performance will be obtained by means of both L1-CAMP and L1-ECS-BAS-CAMP methods. In addition, similar to the plots shown in Fig. 10, the proposed method also suppresses the noise and clutter efficiently compared to MF based algorithm with TBR being $34.02\ \text{dB}\ (\text{SCNR} = -5\ \text{dB}), 43.38\ \text{dB}\ (\text{SCNR} = 0\ \text{dB}), 51.10\ \text{dB}\ (\text{SCNR} = 5\ \text{dB})$, while has a similar effect of image performance improvement as L1-CAMP. In Fig. 12, we find that when $\text{SCNR} \geq -5$ dB, considered scene will be recovered successfully, and the value of SCNR will not influence the required iterative steps (about 10 in this experiment) for the convergence of our proposed method. Since each circle in L1-ECS-BAS-CAMP has a similar computational time, thus there are nearly no difference in convergence speed of L1-ECS-BAS-CAMP under different SCNRs. This means that the existing noise and clutter will not affect the convergent time of our proposed method. Certainly, above analysis between SCNR and computational time is also adapt for L1-CAMP.

D. Performance Versus Down-sampling Ratio and SCNR

To comprehensively compare ECS-BAS, L1-CAMP, and our proposed L1-ECS-BAS-CAMP methods in image performance improvement, we made several experiments based on the different combination of down-sampling ratio δ and SCNR, and use TBR, PSLR, and ISLR as the evaluation criterion of the reconstructed image quality. Simulated scene is identical to the last subsection. In order to illustrate our purpose easily and clearly, without lose of generality, we only performed the random down-sampling along the azimuth direction based on the value of δ, and exploited azimuth PSLR and ISLR to gauge the image quality quantitatively. Table IV shows the value of TBR, PSLR, and ISLR in the ECS-BAS, L1-CAMP, and L1-ECS-BAS-CAMP recovered images under different combination of SCNR and down-sampling ratio. We know that the down-sampling of echo data will cause the azimuth energy dispersion in MF results. This phenomenon corresponds to the increase of ISLR in ECS-BAS recovered images as shown in Table IV, and finally result in the failed reconstruction. While regularization based algorithms also can recover the considered scene accurately even only with $25\ \%$ azimuth data and $\text{SCNR} = -10$ dB. In Table IV, we can see that compared with ECS-BAS, the proposed method suppresses the noise and clutter efficiently with decreasing TBR at least 25 dB, reduces sidelobes dramatically with debasing ISLR more than 45 dB, and also shows a better robustness. In addition, Table IV depicts that L1-ECS-BAS-CAMP has a similar effect in image performance improvement as conventional L_1 regularization imaging technique, no matter what kind of combination of δ and SCNR is set, which is accorded with the results in Fig. 10.

VII. RECONSTRUCTION OF COMPLICATED SCENE

It is known that conventional L_1 regularization SAR imaging technique only can be applied to the recovery of sparse scene because of the restriction of RIP condition and is not appropriate for the non-sparse region, *e.g.*, urban area. However, our proposed azimuth-range decouple L_1 regularization TOPS SAR imaging mechanism introduces a novel idea in the regularization-based reconstruction of non-sparse surveillance region via full-sampled echo data, while does not need to

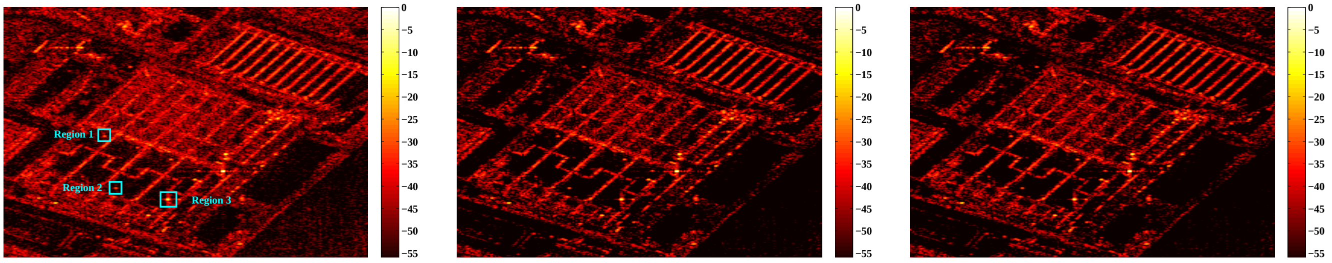

(a) (b) (c)

Fig. 13. Reconstructed image of non-sparse considered scene by different methods. (a) ECS. (b) L1-ECS-BAS-CAMP (Sparse image). (c) L1-ECS-BAS-CAMP (Non-sparse image).

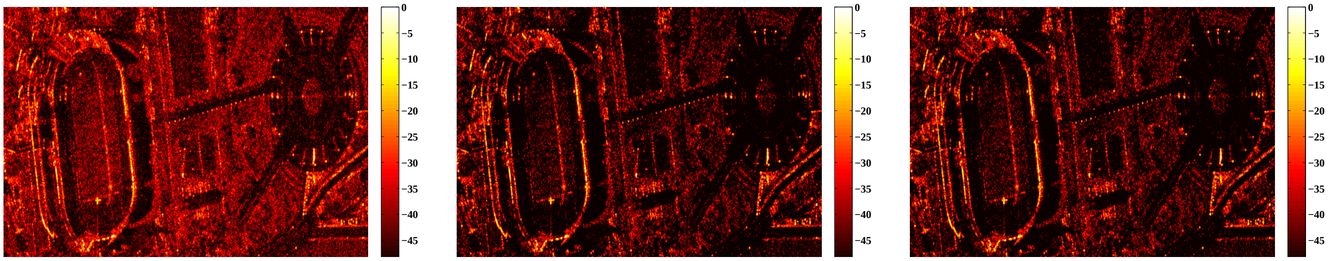

(a) (b) (c)

Fig. 14. Reconstructed image of non-sparse considered scene by different methods. (a) ECS. (b) L1-ECS-BAS-CAMP (Sparse image). (c) L1-ECS-BAS-CAMP (Non-sparse image).

TABLE V
TBR IN THE RECOVERED IMAGE OF NON-SPARSE CONSIDERED SCENE

Region	**Region 1**	**Region 2**	**Region 3**
ECS-BAS	27.90 dB	29.32 dB	26.31 dB
L1-ECS-BAS-CAMP (Sparse image)	36.00 dB	35.04 dB	34.63 dB
L1-ECS-BAS-CAMP (Non-sparse image)	35.95 dB	35.02 dB	34.57 dB

consider the scene sparsity. To validate this, in this section, we set two complicated scenes as the simulated observed regions which points' position and amplitude are set based on the real TerraSAR-X Spotlight SAR image data. Simulation parameters are identical to Table I.

Fig. 13 and Fig. 14 show the recovered image of two simulated non-sparse scenes (urban area) by using ECS and L1-ECS-BAS-CAMP algorithms, respectively. Fig. 13(b) and Fig. 14(b) are the sparse estimations, while Fig. 13(c) and Fig. 14(c) are the non-sparse solutions of our proposed method. Experimental results depict that the proposed method also recovers the non-sparse urban surveillance region well, and suppresses sidelobes and clutter efficiently. In addition, it can be seen that the sparse and non-sparse solutions of L1-ECS-BAS-CAMP have a similar image features. Let us consider three regions indicated by the cyan rectangles in Fig. 13. TBR of these regions are shown in Table V, which results validate the effectiveness of L1-ECS-BAS-CAMP in noise and clutter suppression not only for sparse scenes as above discussion, but also for non-sparse surveillance regions.

VIII. CONCLUSION

This paper proposed a novel azimuth-range decouple based L_1 regularization TOPS SAR imaging mechanism, and successfully applied it to the sparse reconstruction of large-scale considered scene from raw data. In the proposed method, we first exploit the echo simulation operator constructed based on ECS-BAS to replace the exact observation matrix in conventional L_1 regularization based TOPS SAR imaging so as to decouple the azimuth-range couple in raw data, and then reconstruct the considered scene by means of CAMP algorithm. Compared to MF based TOPS SAR imaging technique, *e.g.*, ECS-BAS, L1-ECS-BAS-CAMP provides the improved image performance like significant sidelobes and clutter suppression, and shows a better down-sampled data based imaging ability. Compared with conventional L_1 regularization technique, since it decouples azimuth-range couple well, L1-ECS-BAS-CAMP significantly reduces the computational time and memory occupation in image reconstruction, while providing the similar image features. Furthermore, compared to other recovery algorithms for solving the L_1 regularization problem, CAMP based algorithm provides the sparse image of the considered scene as well as a non-sparse estimation with similar background statistical properties as MF based result, which is very helpful for the further image statistical properties based applications.

In addition, it should be noted that this method makes large-scale sparse TOPS SAR imaging become possible, and also can be used to the recovery of non-sparse surveillance region. Furthermore, in practical TOPS system design, we can increase the swath width through reducing PRF, and use our presented mechanism to achieve the image focusing.

REFERENCES

[1] J. C. Curlander and R. N. Mcdonough, "Synthetic aperture radar: System and signal processing." New York, NY, USA: Wiley, 1991.

[2] F. De Zan and A. M. Guarnieri, "TOPSAR: Terrain observation by progressive scans," *IEEE Trans. Geosci. Remote Sens.*, vol. 44, no. 9, pp. 2352-2360, Sep. 2006.

[3] F. De Zan, "Terrain observation by progressive scans (TOPS-) SAR," in *Proc. European Conference of Synthetic Aperture Radar (EUSAR2008)*, Friedrichshafen, Germany, 2008.

[4] R. K. Moore, J. P. Claassen, and Y. Lin, "Scanning spacebome synthetic aperture radar with integrated radiometer," *IEEE Trans. Aero. Elec. Sys.*, vol. AES-17, pp. 410-421, 1981.

[5] P. Prats, R. Scheiber, J. Mittermayer, A. Meta, and A. Moreira, "Processing of sliding spotlight and TOPS SAR data using baseband azimuth scaling," *IEEE Trans. Geosci. Remote Sens.*, vol. 48, no. 2, pp. 770-780, Feb. 2010.

[6] I. G. Cumming and F. H. Wong, "Digital processing of synthetic aperture radar data: Algorithms and implementation." Norwood, MA, USA: Artech House, 2004.

[7] R. K. Raney, H. Runge, R. Bamler, I. G. Cumming, and F. H. Wong, "Precision SAR processing using chirp scaling," *IEEE Trans. Geosci. Remote Sens.*, vol. 32, no. 4, pp. 786-799, Jul. 1994.

[8] O. Loffeld, A. Hein, and F. Schneider, "SAR focusing: Scaled inverse Fourier transformation and chirp scaling," in *Proc. Int. Geoscience and Remote Sensing Symp. (IGARSS1998)*, vol. 2, pp. 630-632, Seattle. WA, Jul. 1998.

[9] W. Hong, J. Mittermayer, and A. Moreira, "High squint angle processing of E-SAR stripmap data," in *Proc. European Conference of Synthetic Aperture Radar (EUSAR2000)*, Munich, Germany, 2000.

[10] W. G. Carrara, R. S. Goodman, and R. M. Majewski, "Spotlight synthetic aperture radar: Signal processing algorithms." Norwood, MA, USA: Artech House, 1995.

[11] J. Mittermayer, A. Moreira, and O. Loffeld, "Spotlight SAR data processing using the frequency scaling algorithm," *IEEE Trans. Geosci. Remote Sens.*, vol. 37, no. 5, pp. 2198-2214, Sep. 1999.

[12] A. Moreira, J. Mittermayerr, and R. Scheiber, "Extended chirp scaling algorithm for air- and spaceborne SAR data processing in stripmap and ScanSAR imaging modes," *IEEE Trans. Geosci. Remote Sens.*, vol. 34, no. 5, pp. 1123-1136, Sep. 1996.

[13] M. Sack, M. R. Ito, and I. G. Cumming, "Application of efficient linear fm matched filtering algorithms to sar processing," *IEE Proc -F*, vol. 132, no. 1, pp. 45-37, 1985.

[14] J. Mittermayer and A. Moreira, "A generic formulation of the extended chirp scaling algorithm (ECS) for phase preserving ScanSAR and Spot-SAR processing," in *Proc. Int. Geoscience and Remote Sensing Symp. (IGARSS2000)*, vol. 1, pp. 108-110, Honolulu, HI, Jul. 2000.

[15] A. Meta, J. Mittermayer, P. Prats, R. Scheiber, and U. Steinbrecher, "TOPS imaging with TerraSAR-X: Mode design and performance analysis," *IEEE Trans. Geosci. Remote Sens.*, vol. 48, no. 2, pp. 759-769, Feb. 2010.

[16] X. Bai, J. Sun, and W. Hong, "On the TOPS mode spaceborne SAR," *Sci. China Inf. Sci.*, vol. 53, no. 2, pp. 367-378, Feb. 2010.

[17] G. Engen and Y. Larsen, "Efficient full aperture processing of TOPS mode data using the moving band chirp Z-transform," *IEEE Trans. Geosci. Remote Sens.*, vol. 49, no. 10, pp. 3688-3693, Oct. 2011.

[18] W. Xu, P. Huang, Y. Deng, J. Sun, and X. Shang, "An efficient approach with scaling factors for TOPS mode SAR data focusing," *IEEE Geosci. Remote Sens. Lett.*, vol. 8, no. 5, pp. 929-933, Oct. 2011.

[19] G. Sun, M. Xing, Y. Wang, Y. Wu, and Z. Bao, "Sliding spotlight and TOPS SAR data processing without sub-sperture," *IEEE Geosci. Remote Sens. Lett.*, vol. 8, no. 6, pp. 1036-1040, Nov. 2011.

[20] W. Xu, P. Huang, R. Wang, Y. Deng, and Y. Lu, "TOPS-mode raw data processing using chirp scaling algorithm," *IEEE Trans. Geosci. Remote Sens.*, vol. 7, no. 1, pp. 235-246, Jan. 2014.

[21] D. L. Donoho, "Compressed sensing," *IEEE Trans. Inf. Theory*, vol. 52, no. 4, pp. 1289-1306, Apr. 2006.

[22] E. T. Candès and T. Tao, "Near-optimal signal recovery from random projections: Universal encoding strategies," *IEEE Trans. Inf. Theory*, vol. 52, no. 12, pp. 5406-5425, 2006.

[23] E. T. Candès, J. Romberg, and T. Tao, "Stable signal recovery from incomplete and inaccurate measurements," *Commun. Pur. Appl. Math.*, vol. 59, no. 8, pp. 1207-1223, 2006.

[24] H. Nyquist, "Certain topics in telegraph transmission theory," *Trans. Amer. Inst. Electrial Engining*, vol. 47, no. 2, pp. 617-644, Jul. 1928.

[25] C. E. Shannon, "Communication in the presence of noise," in *Proc. IRE*, vol. 37, no. 1, pp. 10-21, 1949.

[26] R. Baraniuk and P. Steeghs, "Compressive radar imaging," in *Proc. IEEE Radar Conference*, Boston, MA, 2007. pp. 128-133.

[27] X. X. Zhu and R. Bamler, "Tomographic SAR inversion by L_1-norm regularization-the compressive sensing approach," *IEEE Trans. Geosci. Remote Sens.*, vol. 48, no. 10, pp. 3835-3846, 2010.

[28] L. Zhang, M. Xing, C. Qiu, J. Li, and Z. Bao, "Achieving higher resolution ISAR imaging with limited pulses via compressed sampling," *IEEE Geosci. Remote Sens. Lett.*, vol. 6, no. 3, pp. 567-571, 2009.

[29] Y. Yu, A. Petropulu, and H. Poor, "MIMO radar using compressive sampling array processing," *IEEE J. Sel. Topics Signal Process.*, vol. 4, no. 1, pp. 146-163, 2010.

[30] B. Zhang, W. Hong, and Y. Wu, "Sparse microwave imaging: Principles and applications," *Sci. China Inf. Sci.*, vol. 55, no. 8, pp. 1-33, 2012.

[31] M. Çetin, I. Stojanovic, N. Önhon, K. Varshney, S. Samadi, W. C. Karl, and A. S. Willsky, "Sparsity-driven synthetic aperture radar imaging: Reconstruction, autofocusing, moving targets, and compressed sensing," *IEEE Signal Process. Mag.*, vol. 31, no. 4, pp. 27-40, 2014.

[32] L. Zhao, L. Wang, L. Yang, A. M. Zoubir, and G. Bi, "The Race to improve radar imagery: An overview of recent progress in statistical sparsity-based techniques," *IEEE Signal Process. Mag.*, vol. 33, no. 6, pp. 85-102, 2016.

[33] J. Fang, Z. Xu, B. Zhang, W. Hong, and Y. Wu, "Fast compressed sensing SAR imaging based on approximated observation," *IEEE J. Sel. Topics Appl. Earth Obs. Remote Sens.*, vol. 7, no. 1, pp. 352-363, 2014.

[34] H. Bi, B. Zhang, X. X. Zhu and W. Hong, "Azimuth-range decouple-based L_1 regularization method for wide ScanSAR imaging via extended chirp scaling," *J. Appl. Remote Sens.*, vol. 11, no. 1, pp. 015007:1-12, 2017.

[35] D. L. Donoho, A. Maleki, and A. Montanari, "Message passing algorithms for compressed sensing," *Proc. Nat. Acad. Sci.*, vol. 106, no. 45, pp. 18914-18919, 2009.

[36] A. Maleki, L. Anitori, Z. Yang, and R. Baraniuk, "Asymptotic analysis of complex LASSO via complex approximate message passing (CAMP)," *IEEE Trans. Inf. Theory*, vol. 59, no. 7, pp. 4290-4308, 2013.

[37] L. Anitori, A. Maleki, M. Otten, R. Baraniuk, and P. Hoogeboom "Design and analysis of compressed sensing radar detectors," *IEEE Trans. Signal process*, vol. 61, no. 4, pp. 813-827, 2013.

[38] I. Daubechies, M. Defriese, and C. De Mol, "An iterative thresholding algorithm for linear inverse problems with a sparsity constraint," *Commun. Pure Appl. Math.*, vol. LVII, pp. 1413-1457, 2004.

[39] J. A. Tropp, "Greed is good: Algorithmic results for sparse approximation," *IEEE Trans. Inf. Theory*, vol. 50, no. 10, pp. 2231-2242, 2004.

[40] R. Tibshirani, "Regression shrinkage and selection via the LASSO," *J. Roy. Stat. Soc., Series B*, vol. 58, no. 1, pp. 267-288, 1996.

[41] M. Çetin, W. C. Karl, and D. A. Castanon, "Feature enhancement and ATR performance using nonquadratic optimization-based SAR imaging," *IEEE Trans. Aero. Elec. Sys.*, vol. 39, no. 4, pp. 1375-1395, 2003.

Hui Bi was born in 1991 in Shandong, China. He received the Bachelor degree in Electronics and Information Engineering from YanTai University, Yantai, China, in 2012. Since September 2012, he has been working to the Ph.D. degree in the University of Chinese Academy of Sciences (UCAS). Now he is also working in the Science and Technology on Microwave Imaging Laboratory, Institute of Electronics, Chinese Academy of Sciences (IECAS), Beijing, China. His main research interests are sparse microwave imaging with compressive sensing, synthetic aperture radar data processing and application, sparse signal processing, and tomographic synthetic aperture radar imaging.

Bingchen Zhang was born in 1973. He received the Bachelor degree in Electronic Engineering and Information Science from the University of Science and Technology of China (USTC), 1996, the master degree in the Institute of Electronics, University of the Chinese Academy of Sciences, Beijing in 1999. Since 1999, he has been working in the Institute of Electronics, Chinese Academy of Sciences as a Scientist. His main research interests are sparse microwave imaging, synthetic aperture radar, radar signal processing and radar system.

Xiao Xiang Zhu (S10-M12-SM14) received the bachelor degree in space engineering from the National University of Defense Technology (NUDT), Changsha, China, in 2006. She received the Master (M.Sc.) degree, her doctor of engineering (Dr.-Ing.) degree and her Habilitation in the field of signal processing from Technical University of Munich (TUM), Munich, Germany, in 2008, 2011 and 2013, respectively.

Since 2011, she is a scientist with the Remote Sensing Technology Institute at the German Aerospace Center (DLR), Oberpfaffenhofen, where she is the head of the Team Signal Analysis. Since 2013, she is also a Helmholtz Young Investigator Group Leader and appointed as TUM junior fellow. In 2015, she is appointed as the Professor for Signal Processing in Earth Observation at TUM. Prof. Zhu was a guest scientist or visiting professor at the Italian National Research Council (CNR-IREA), Naples, Italy, Fudan University, Shanghai, China, the University of Tokyo, Tokyo, Japan and University of California, Los Angeles, United States in 2009, 2014, 2015 and 2016, respectively. Her main research interests are: advanced InSAR techniques such as high dimensional tomographic SAR imaging and SqueeSAR; computer vision in remote sensing including object reconstruction and multi-dimensional data visualization; big data analysis in remote sensing, and modern signal processing, including innovative algorithms such as sparse reconstruction, nonlocal means filter, robust estimation and deep learning, with applications in the field of remote sensing such as multi/hyperspectral image analysis.

Dr. Zhu is an associate Editor of IEEE Transactions on Geoscience and Remote Sensing.

Chenglong Jiang was born in Fujian, China, in 1987. He received B.S. degree in electronic engineering and information science from University of Science and Technology of China (USTC) in 2009, and the Ph.D. degree in signal and information processing from University of Chinese Academy of Sciences (UCAS) in 2015. From 2009 to 2015, he worked in the Science and Technology on Microwave Imaging Laboratory, Institute of Electronics, Chinese Academy of Sciences, China. His current research interests include sparse signal processing and its applications to microwave imaging and radar signal processing.

Wen Hong was born in 1968. She received the Ph.D. degree from Beijing University of Aeronautics and Astronautics (BUAA), Beijing, China, in 1997. She was with the Department of Electrical Engineering, BUAA, as a Faculty Member in signal and information processing from 1997 to 2002. In between, she worked with the DLR-HF, Wessling, Germany, as a Guest Scientist from 1998 to 1999 for one year. Since 2002, she has been working in the Science and Technology on Microwave Imaging Laboratory as a Scientist. Her main research interests are polarimetric/polarimetric interferometric synthetic aperture radar data processing and application, 3-D SAR signal processing, circular SAR signal processing and sparse microwave imaging with compressed Sensing.